NASA TECHNICAL MEMORANDUM

NASA TM X-3267

NASA TM X-3267

EFFECT OF A 180°-EXTENT INLET PRESSURE DISTORTION ON THE INTERNAL FLOW CONDITIONS OF A TF30-P-3 ENGINE

Claude E. de Bogdan, John H. Dicus,
David G. Evans, and Ronald H. Soeder

Lewis Research Center
Cleveland, Ohio 44135

NATIONAL AERONAUTICS AND SPACE ADMINISTRATION • WASHINGTON, D. C. • SEPTEMBER 1975

1. Report No.	2. Government Accession No.	3. Recipient's Catalog No.
NASA TM X-3267		

4. Title and Subtitle	5. Report Date
EFFECT OF A 180°-EXTENT INLET PRESSURE DISTORTION ON THE INTERNAL FLOW CONDITIONS OF A TF30-P-3 ENGINE	September 1975
	6. Performing Organization Code
7. Author(s)	8. Performing Organization Report No.
Claude E. de Bogdan, John H. Dicus, David G. Evans, and Ronald H. Soeder	E-8206
	10. Work Unit No. 505-05
9. Performing Organization Name and Address	11. Contract or Grant No.
Lewis Research Center National Aeronautics and Space Administration Cleveland, Ohio 44135	
	13. Type of Report and Period Covered
12. Sponsoring Agency Name and Address	Technical Memorandum
National Aeronautics and Space Administration Washington, D.C. 20546	14. Sponsoring Agency Code

15. Supplementary Notes

16. Abstract

The measured effects of inlet pressure distortion on the internal flow temperatures and pressures of a Pratt & Whitney TF30-P-3 afterburning turbofan engine are reported. Extensive inner-stage instrumentation combined with stepwise rotation of pressure distortion provided a high degree of circumferential resolution in the data. The steady-state spatial variation in pressures, temperature, and calculated flow velocity and the amplitude and extent of the distorted sectors are given. Data are presented for runs of 77 and 90 percent of low-speed-rotor design speed at pressure distortion levels two-thirds of that required to stall the engine. These data are compared with data taken at clean-inlet conditions. Results indicate that the inlet pressure distortion was quickly attenuated within the compressor, except at the hub of the low-pressure compressor. The distorted sectors also swirled and varied in extent as they passed through the engine. Average velocities within the compressor were about equal to the clean-inlet values.

17. Key Words (Suggested by Author(s))	18. Distribution Statement
Turbofan Inlet flow distortion Airjets Compressor stall	Unclassified - unlimited STAR Category 07 (rev.)

19. Security Classif. (of this report)	20. Security Classif. (of this page)	21. No. of Pages	22. Price*
Unclassified	Unclassified	63	$4.25

* For sale by the National Technical Information Service, Springfield, Virginia 22161

EFFECT OF A 180°-EXTENT INLET PRESSURE DISTORTION ON THE INTERNAL FLOW CONDITIONS OF A TF30-P-3 ENGINE

by Claude E. de Bogdan, John H. Dicus, David G. Evans, and Ronald H. Soeder

Lewis Research Center

SUMMARY

The measured effects of inlet pressure distortion on the internal flow temperatures and pressures of a Pratt & Whitney TF30-P-3 afterburning turbofan engine are reported. Extensive inner-stage instrumentation combined with stepwise rotation of pressure distortion provided a high degree of circumferential resolution in the data. The steady-state spatial variation in pressures, temperature, and calculated flow velocity and the amplitude and extent of the distorted sectors are given. Data are presented for runs of 77 and 90 percent of low-speed-rotor design speed at pressure distortion levels two-thirds of that required to stall the engine. These data are compared with data taken at clean inlet conditions. Results indicate that the inlet pressure distortion was quickly attenuated within the compressor, except at the hub of the low-pressure compressor. The distorted sectors also swirled and varied in extent as they passed through the engine. Static pressure distortion was attenuated by the large passage volumes at the fan and compressor exits, with a resulting decrease in total pressure distortion in these areas. The overall performance of the compressor system with a distorted inlet did not change substantially from its clean-inlet performance.

Contained in this report are curves showing, for each measuring station, the attenuation (amplification in the case of total temperature) and swirl of the total and static pressure, total temperature, and calculated flow velocity variations within the compressor system. The spatial relationship among the total pressure, static pressure, and temperature distortions that are present within the compressor is shown at various measuring stations. Curves are also presented which compare the average flow velocities obtained with and without inlet distortion at each measuring station. Detailed plots of internal pressures, temperatures, calculated velocities, and average Mach numbers are presented in an appendix to this report.

INTRODUCTION

A TF30-P-3 engine was installed in the Lewis Research Center Propulsion Systems Laboratory altitude test facility and experimentally operated with square-wave inlet pressure distortion. Circumferential and radial pressures and temperatures were recorded at measuring stations within the compressor and at the turbine exit. To date, much of the work relating the effects of inlet flow distortion to engine performance has dealt primarily with the overall measurement of engine stability. However, in order to better understand the effects of inlet distortion on engine stability, there is a need to determine the flow mechanism and adjustments that occur within the compressor system. This information can also provide a basis for developing modeling techniques to predict analytically the behavior of compressor systems with distorted flow. One such technique is the parallel-compressor approach noted in reference 1.

Because of various limiting factors, such as data recording system capacity and space limitations within the compressor, the amount of instrumentation placeable within a compressor is usually insufficient to provide a complete spatial representation of the flow properties. One of the most common shortcomings is inadequate circumferential coverage of instrumentation at each measuring station. Therefore, a test was conducted in which the distortion generated by an air-jet distortion device was rotated at the inlet of the TF30-P-3 engine. Rotating the distortion past the instrumentation rakes produced the same effect as increasing the circumferential coverage of the instrumentation at each measuring station.

Flow measurements taken within the compressor system and at the turbine exit were used to determine (1) the spatial variation of flow pressures, temperatures, and velocities, (2) the attenuation and rotation characteristics of the distorted sector, and (3) the characteristics of the temperature distortion resulting from the pressure distortion. These effects were determined from steady-state data taken at two nominal low-speed-rotor speeds: 7400 and 8600 rpm (approx. 77 and 90 percent of design speed) at a Reynolds number index of 0.5. Preliminary results obtained at the higher speed are reported in reference 2.

The work reported herein was done in the U.S. customary system of units. Conversion to the International System of Units (SI) was for reporting purposes only.

SYMBOLS

M Mach number

N speed of rotation, rpm

P pressure, N/m^2

T	absolute total temperature, K
V	flow velocity, m/sec
W	mass flow rate, kg/sec
γ	ratio of specific heats
δ	ratio of total pressure to sea-level total pressure
η	efficiency, $\left[\left(\frac{P_{T,4}}{P_{T,2}}\right)^{(\gamma-1)/\gamma} - 1\right] \Big/ \left[\left(\frac{T_4}{T_2}\right) - 1\right]$ or $\left[\left(\frac{P_{T,2.3f}}{P_{T,2}}\right)^{(\gamma-1)/\gamma} - 1\right] \Big/ \left[\left(\frac{T_{2.3f}}{T_2}\right) - 1\right]$
θ	ratio of total temperature to sea-level total temperature
μ	absolute viscosity, (kg)(sec)/cm
φ	ratio of absolute viscosity to sea-level absolute viscosity

Subscripts:

a	air
C	core
F	fan
f	face
H	high-speed rotor
L	low-speed rotor
max	maximum
min	minimum
r	ring
S	static
sl	sea-level standard conditions
T	total
2, 2.3, 3, etc.	station locations (fig. 2)

Superscript:

(–)	average

APPARATUS, INSTRUMENTATION, AND TEST PROCEDURE

Apparatus

The engine used in these tests was a TF30-P-3 twin-spool turbofan installed in an altitude test chamber. Both engine and chamber are described in reference 3.

Distortion in inlet total pressure was generated by an NASA-developed air-jet device (ref. 4). This device produces total pressure distortion patterns by injection of additional secondary air into the inlet passage in the direction opposite to the primary flow. Both the device and the engine compression system are shown schematically in figure 1. The device contains 54 individual jets divided into six 60° sectors of nine jets each. A remotely controlled, hydraulically driven valve independently governs the flow to each sector. The degree of pressure suppression (distortion) is controlled by this flow.

Instrumentation

The properties measured were total and static pressure and total temperature. Station identification, probe location, and probe type (high response and steady state) are shown in figure 2. Although only steady-state data are reported herein, high-response transient data were recorded and high-response instrumentation locations are shown for information only. Circumferential probe positions in degrees and radial probe locations in percentage of passage height are given in table I. The steady-state data acquisition systems are fully described in reference 5. High-response transient instrumentation is discussed in reference 6.

Procedure

The engine was operated at two nominal speeds (77 and 90 percent of low-speed-rotor design) with a 180° inlet distortion and a Reynolds number index of 0.5. Calculated operating parameters at these conditions are compared to clean-inlet and stall conditions in table II.

Distortion runs were made by using the same flow through three adjacent 60° air-jet sectors to give a 180° distortion. The 180° distortion was then indexed circumferentially in 60° steps. The distortion amplitude was held constant at approximately two-thirds of the amplitude required to stall the engine. Steady-state data were taken at each 60° step. This procedure effectively multiplied the amount of instrumentation by a factor of 6, thus greatly increasing the circumferential resolution of the data at each station. The resulting total and static pressure inlet distortion measured at station 2 is given in figure 3.

The engine was then brought to stall conditions by increasing the distortion amplitude in the 0^{o} to 180^{o} position. Inlet distortion amplitude at stall was approximately 13 percent at 8600 rpm and 9 percent at 7400 rpm.

RESULTS

The radially averaged total pressure and static pressure distortion patterns at the inlet (station 2) are given in figure 3. Note the close circumferential spacing of the data resulting from the stepwise rotation of the inlet distortion. Nominally, the distortion amplitude $(P_{T,max} - P_{T,min})/P_{T,av}$ was held at 9 percent for 8600 rpm and at 6 percent for 7400 rpm. The air-jet system produced very nearly a square wave in total pressure distortion, with a resulting sinusoidal static pressure pattern. The static pressure distortion built up rapidly such that total and static pressure distortion amplitudes were approximately equal at station 2.1 (behind first fan stage).

Plots of circumferential variation in P_T, P_S, T, V, and M at each station for both speeds are given in figures 13 to 18 (appendix, p. 31). A more general presentation of the data is given in figures 4 to 12, a discussion of which follows.

Figure 4 shows the extent and circumferential position of the distorted (below average) P_T segment as it passed through the compressor system. The ring-averaged distortion level for each station is also plotted in figure 4. Inlet distortion amplitude for the high-speed run (fig. 4(b)) was approximately twice that of the low-speed run (fig. 4(a)), but both showed essentially similar trends. The distortion amplitude in the fan tip annulus (stations 2 to 2.6f) attenuated faster than that in the fan hub annulus (stations 2 to to 2.3), and tip and mean values decreased fairly steadily through the low-pressure compressor (stations 2.3 to 3). However, the hub profiles show a distortion level at the exit of the low-pressure compressor (LPC) that is approximately equal to the inlet value; that is, a small drop from 7 percent to 6.1 percent between stations 2 and 3 at 8600 rpm and an increase from 3 percent to 4 percent at 7400 rpm. It may be argued that the hub distortion was attenuated at station 2.6 and then amplified at station 3, possibly because of localized effects, such as hub-cavity crossflows, or the hub pumping characteristics. But it is impossible to be certain since there are no hub data for station 2.6. However, it appears more likely that the LPC was simply unable to dissipate pressure distortion at the hub throughout its length. Once into the high-pressure compressor (HPC), station 3.12, the distortion at the hub was rapidly diminished to the level of that at the tip (about 2 percent for 7400 rpm and 3 percent for 8600 rpm). The distortion level was down to 1.5 percent for both speeds at the HPC exit (station 4).

The circumferential extent of the region at lower pressure than the ring-averaged total pressure, station by station, is shown in figure 4(b) for 8600 rpm. Here the

distortion for tip and mean probes rotated 50° counterclockwise (opposite to the direction of rotation) as it moved back to station 2.6. There it reversed and expanded in extent to give a net clockwise rotation at the LPC exit (station 3). Again, the lack of hub data at station 2.6 clouds the picture, but the LPC appeared to swirl the hub area distortion clockwise from the inlet and then concentrate it in the span between 105° and 245°. The distortion concentration at the hub in the HPC (shaded area in the figure) continued to rotate counterclockwise, diminishing in amplitude, as it moved back to station 4. The distortion at station 3.12 for mean and tip positions (no hub data taken for this station) formed into two areas of low amplitude. The area to the right continued to swirl to the right, while the area to the left narrowed and moved to the left as it approached the HPC exit. The low-speed run (fig. 4(a)) shows essentially the same behavior.

Static pressure distortion (fig. 5) built up in the fan stream from the inlet to station 2.1 then attenuated to less than 1 percent at station 2.6f for the low-speed run. In the high-speed run, distortion built up to twice that of the low-speed run but decayed at a greater rate and was nonexistent at station 2.6f. It is assumed that the rapid decrease in amplitude in the fan stream was due to the effect of the large passage volume downstream of station 2.6. Behavior of the static pressure distortion in the core stream, in general, followed the same pattern as did the total pressure. The distorted area also broke up into two zones in the HPC. The two zones were already evident at the entrance to the HPC (station 3) for the high-speed run.

Because several annular cavities opened to the compressor flow path at the hub (stations 2.1, 2.3, and 3), it was assumed that the circumferential variation in static pressures shown in figure 5 can cause circumferential flow (crossflow) within these cavities. The reentry of these crossflows to the compressor flow path on the low-static-pressure side of a distorted annulus has been known to cause distortion amplification in fans and compressors. However, the hub amplification of total pressure noted at station 3 may not be due to this effect; as may be noted in figure 5, the circumferential location of minimum static pressure extended beyond that of the hub amplification region noted in figure 4.

A comparison of figures 4 and 5 shows that the amplitudes of total and static pressure distortion at the fan and the exits of the LPC and HPC were approximately equal at 7400 rpm. At 8600 rpm, however, the static pressure distortion amplitude was about one-half of the total pressure distortion amplitude at the fan and LPC exits and equal at the HPC exit.

The spatial variation of total temperature distortion for both runs is given in figure 6. Ideally, there should have been zero temperature distortion at the inlet. However, the temperature of the air feeding the air-jet distortion device was higher than the inlet air by about 1 deg C (1.5 deg F) for the high-speed run and about 0.5 deg C (0.75 deg F) for the low-speed run. This temperature error is represented by the apparent offset of the distorted area and was negative with respect to the normally expected temperature

distortion buildup. As shown in figure 6, the distortion level built rapidly back to station 2.6 for the high-speed run and to station 3 for the low-speed run. There was no further increase back through the compressors until the tip area of station 4. The circumferential extent of temperature distortion apparently did not rotate until the final stages of the HPC. The fan tip region showed a slightly higher distortion level than the hub for both runs.

For comparison with the observed values, the total temperature distortion amplitude was calculated based on the circumferential variation in pressure ratio (and hence in heat of compression) across major stage groups. The results did not compare well. The calculated temperature distortion amplitude in the fan, hub, LPC, and HPC showed a minimum buildup in the front of the engine and a maximum value some 30 percent below that measured.

The spatial variation in velocity distortion calculated for both runs is mapped in figure 7. (In this report, the word velocity always means flow velocity.) Values are based on tip static pressure everywhere except stations 2, 2.3f, and 2.6f. Distortion levels in flow velocity were similar for both runs, particularly in the first three stages (up to stations 2.3 and 2.3f). For the low-speed run, hub, tip, and mean values for station 2.1, as well as hub values for station 2.3, were greater than those of the high-speed run. Levels through the remainder of the engine at 8600 rpm were about 30 percent greater than those at 7400 rpm. Velocity distortion amplification seemed to occur more easily at the lower speed, where it is seen at the hub and tip for station 2.1 and at the tip for station 4.

The circumferential variation of velocity distortion was complex. At 7400 rpm the initial 180° input distortion expanded to two lobes at station 2.1 then contracted to the original 180° at station 2.3f and once again broke into two lobes at the exit. (The calculated two-lobe velocity distortion patterns were possibly caused by the difference in the rate of rotation and attenuation of the total and static pressure defect areas.) The pattern at 8600 rpm was similar but more compact. There was only one two-lobe area, that at station 2.1, and the net circumferential travel was only 30° in the direction of rotor rotation, compared to 120° for 7400 rpm.

Figure 8 shows the radial variation of total pressure distortion defined as $P_{T,max} - P_{T,min}$ for the ring, divided by the face-averaged total pressure for the station. (Face-averaged values of P_T, P_S, T, and V at each station are given in table III.) The ring radii are plotted on the ordinate, and the percentage of distortion for each ring is plotted on the abcissa. For clarity, the annulus heights are shown to scale. The radial variation in distortion is easily seen from the plot. With the exception of stations 2.6 and 3.12, the variation is similar for both speeds. Most noticable are the distortion amplification at the hub of station 3 and the radial variation in inlet distortion at station 2.

Both radial and circumferential distribution for P_T, T, and V distortions are shown in the polar plots of figure 9. The circumferential extent of P_S distortion is given at the periphery of the total pressure plot. The relative locations of pressure and

temperature probes are plotted at their radial positions in the compressor annuli (shown to scale). The probes were then located circumferentially at the points where the distortion parameters crossed their average values. This series of plots is included to show the relative circumferential position of the three defect areas and also to show how the pure 180° distortion shifts to a radial pattern. Note that the total temperature distortion persisted back to the low-pressure-turbine exit and fan bypass duct (stations 7f and 7g; fig. 9(b)), where the defect areas were out of phase by 180°.

Another view of the rotational behavior of the distorted zones can be seen in figures 10 and 11. Here the relative circumferential positions of the centerlines of the P_T, P_S, T, and V distorted areas are plotted against station axial position (to scale). The calculated streamline path is included for comparison and is based on the design flow velocity diagrams for the compressor system. The fan and core streams are given in two plots apiece for clarity. The calculated streamline path did not show the expected similarity to the temperature path. Nor is there a correlation with any of the measured parameter centerlines.

Station face-averaged flow velocities for both the distorted- and clean-inlet conditions are compared in figure 12. These plots show that the inlet distortion had only a small effect. The distortion runs had a slightly higher average flow velocity (about 4.5 percent for 7400 rpm and 5.5 percent for 8600 rpm) than the clean-inlet runs. The velocities were significantly different only at the exit of the HPC, where the average flow velocity with a distorted inlet fell below the clean-inlet value by about 20 percent.

Calculated operating parameters are compared in table IV for clean- and distorted-inlet conditions. Here also the inlet distortion levels of these tests had little effect on operating efficiency.

SUMMARY OF RESULTS

The effect of operating the TF30-P-3 turbofan engine with 180° distortion in inlet total pressure on the flow conditions measured within the compressor system at low-speed-rotor speeds of 7400 rpm and 8600 rpm are summarized as follows:

1. The air-jet distortion device used produced a nearly square-wave profile in total pressure and flow velocity at the inlet, with some dropoff in amplitude at the inner radius of the inlet annulus. The corresponding circumferential profile in static pressure was sinusoidal.

2. A large buildup in static pressure distortion occurred immediately ahead of and within the first stage of the fan. The buildup resulted in a static pressure distortion amplitude at station 2.1 that was approximately equal to the amplitude of total pressure distortion measured at station 2.

3. The amplitudes of the static pressure distortion at the fan and at the low- and high-pressure-compressor exits were equal to the amplitudes of the total pressure distortion measured at these stations at 7400 rpm but varied from 1/2 to 1 times the total pressure distortion amplitude at 8600 rpm.

4. A two-lobe circumferential variation in flow velocity of 5 to 30 percent in amplitude occurred within the second and third fan stages, probably caused by the difference in rate of rotation, attenuation, and shape of the total and static pressure defect areas.

5. The distorted sectors within the compressor system shifted from a purely circumferential distortion at the engine inlet to a mixed circumferential and radial pattern at all measuring stations within the compressor system.

6. The rate at which the distortion in inlet total pressure attenuated within the compressor system increased with increasing rotor speed.

7. Some swirl and variation in the circumferential extent of the distorted sectors occurred within the compressor system. In general, all sectors rotated opposite to rotor rotation back to station 2.3, where they reversed and rotated with the rotor back to the low-pressure-compressor exit. The high-pressure-compressor tended to break the pressure sectors into two zones and to rotate the temperature sector from 40° to 80° in the direction of rotor rotation.

8. The regions of total and static distorted pressure remained approximately coincident throughout the compressor system. However, the region of elevated total temperature overlapped the minimum pressure region by approximately 90° and did not coincide with the calculated particle flow path through the compressor system.

9. The observed variation in total temperature distortion amplitude did not compare well with that calculated based on variation in heat of compression caused by the circumferential variation in compressor pressure ratio.

10. A significant amplitude of circumferential and radial total pressure distortion was present between the low- and high-pressure compressors. The cause was not apparent, but it may be indicative of the presence of crossflows at station 3 or of some blading characteristic in the hub region of the low-pressure compressor.

11. The average flow velocities measured at each station within the compressor system (when operating with inlet distortion) were approximately equal to the velocities measured with a clean inlet.

12. A sinusoidal variation in total temperature was measured at the exit of the low-pressure turbine and fan bypass duct (stations 7f and 7g). The variation between the two stations was out of phase by 180°.

13. The testing technique of rotating the inlet pressure distortion was an effective means of mapping the spatial variation in flow conditions within the engine.

14. The levels of inlet total pressure distortion used in these tests had little effect on the overall operating parameters.

Lewis Research Center,
National Aeronautics and Space Administration,
Cleveland, Ohio, February 27, 1975,
505-05.

REFERENCES

1. Braithwaite, Willis M.; Graber, Edwin J.; and Mehalic, Charles M.: The Effects of Inlet Temperature and Pressure Distortion on Turbojet Performance. AIAA Paper 73-1316, Nov. 1973.

2. Evans, David G.; de Bogdan, Claude E.; Soeder, Ronald H.; and Pleban, Eugene J.: Some Comparisons of the Flow Characteristics of a Turbofan Compressor System with and without Inlet Pressure Distortion. Presented at SQUID/AFOSR/United Aircraft Res. Lab. Workshop on Unsteady Flows in Jet Engines, East Hartford, Conn., July 11-12, 1974.

3. McAulay, John E.; and Abdelwahab, Mahmood: Experimental Evaluation of a TF30-P-3 Turbofan Engine in an Altitude Facility: Afterburner Performance and Engine-Afterburner Operating Limits. NASA TN D-6839, 1972.

4. Meyer, Carl L.; McAulay, John E.; and Biesiadny, Thomas J.: Technique for Inducing Controlled Steady-State and Dynamic Inlet Pressure Disturbances for Jet Engine Tests. NASA TM X-1946, 1970.

5. Central Automatic Data Processing System. NACA TN 4212, 1958.

6. Braithwaite, Willis M.; Dicus, John H.; and Moss, John E., Jr.: Evaluation with a Turbofan Engine of Air Jets as a Steady-State Inlet Flow Distortion Device. NASA TM X-1955, 1970.

7. Dicus, John H.: FORTRAN Program to Generate Engine Inlet Flow Contour Maps and Distortion Parameters. NASA TM X-2967, 1974.

8. Glawe, George E.; Simmons, Fredrick S.; and Stickney, Truman M.: Radiation and Recovery Corrections and Time Constants of Several Chromel-Alumel Thermocouple Probes in High Temperature, High Velocity Gas Streams. NACA TN 3766, 1956.

TABLE I. - POSITION AND TYPE OF INSTRUMENTATION

Engine instrumentation station	Type of instrumentation[a]	Position[b]	Circumferential position, deg	Radial position	
				cm	Percent of passage height
2	P_S	o	22.5	46.56	100
			67.5		
			107.5		
			157.5		
			202.5		
			247.5		
			337.5		
		i	22.5	15.85	0
			107.5		
			202.5		
			287.5		
	P_T	1	0	44.45	95.2
		2		39.88	78.4
		3		34.72	61.5
		4		28.70	41.8
		5		21.01	16.8
	T	1		42.16	87.2
	T	2		31.70	50.7
(c)					
2.1	P_S	o	45	43.97	100
			53		
			258		
			266		
	P_T	1	282	42.04	92.8
		3		33.22	60.2
		4		27.81	40.1
		5		19.20	8.2
	---	Hub	---	17.68	0
	T	1	282	39.95	85.0
		2		35.56	68.8
		3		30.51	50.1
		4		24.46	27.7
2.3	P_S	o	111	28.75	46.2
		o	118	28.75	46.2
		o	246	28.75	46.2
		o	251	28.75	46.2
	P_T	1	88	27.64	41.5
		2		25.22	31.3
		3		22.53	20.0
		4		19.48	7.2
		1	259	27.64	41.5
		2	259	25.20	31.3
		3	259	19.71	7.2
	---	Hub	---	17.17	0
	T	1	56	27.94	42.7
		2		26.26	35.7
		3		24.23	27.2
		4		22.00	17.75
		5		19.51	7.16
		1	259	22.56	20.1

Engine instrumentation station	Type of instrumentation[a]	Position[b]	Circumferential position, deg	Radial position	
				cm	Percent of passage height
2.3f	P_S	i	70	31.19	56.5
		i	282	31.19	56.5
		o	118	41.55	100
		o	238	41.55	100
	P_T	1	111	40.41	95.2
		2		38.00	85.1
		3		35.43	74.3
		4		32.05	60.0
		1	252	36.50	78.8
		2	252	34.72	71.3
	T	1	56	40.51	95.6
		2		38.63	87.7
		3		36.65	79.4
		5		32.33	61.2
		1	252	38.40	86.8
2.6	P_S	o	65	10.26	100
	P_S	o	69	10.26	100
	P_S	o	245	10.26	100
	---	Hub	---	17.68	0
	P_T	1	89	24.89	85.8
	P_T	2	89	22.28	54.7
	T	1	130	25.32	91.0
		2		23.85	73.4
		3		22.25	54.4
		4		20.57	34.5
		5		18.69	12.1
2.6f	P_S	o	120	41.78	100
		i	116	29.90	0
		o	171	41.78	100
		i	171	29.90	0
		o	300	41.78	100
		i	300	29.90	0
		o	352	41.78	100
		i	352	29.90	0
	P_T	1	100	41.61	98.7
		2		41.38	96.6
		3		41.12	94.5
		4		40.87	92.4
		5		39.98	84.9
		6		38.23	70.3
		7		36.42	54.9
		8		34.49	38.7
		9		32.46	21.6
		10		31.34	12.2
		11		30.99	9.2
		12		30.66	6.3
		13		30.33	3.6
	T	1	10	39.90	84.3
		2		38.15	69.5
		3		36.32	54.1
		4		34.42	38.1
		5		32.39	20.9
(d)					

[a]See test for definition of symbols.

[b]Inner annular wall is denoted by i, outer annular wall by o; numbers denote rings.

[c]P_T and T probe arrangement repeated circumferentially every 45°.

[d]P_T probe arrangement repeated at 161°, 286°, and 341°; T arrangement repeated at 259°.

TABLE I. - Concluded.

Engine instrumentation station	Type of instrumentation[a]	Position[b]	Circumferential position, deg	Radial position	
				cm	Percent of passage height
3	P_S	o	81	25.46	100
	P_S	o	297	25.46	100
	P_T	1	117	23.60	85.2
	↓	2	117	21.56	53.8
	↓	3	117	19.35	19.0
	↓	1	261	23.80	88.4
	↓	2	261	22.58	69.5
	↓	3	261	20.40	35.2
	---	Hub	---	18.14	0
	T	1	58	24.00	91.3
	↓	2	↓	22.58	72.7
	↓	3	↓	21.62	54.0
	↓	4	↓	20.27	33.0
	↓	5	↓	18.92	12.0
	↓	1	261	21.44	51.4
	↓	2	261	19.13	15.4
	↓	Avg	226	-----	-----
3.12	P_S	o	72	24.23	100
	↓	↓	75	↓	↓
	↓	↓	285	↓	↓
	↓	↓	288	↓	↓
	P_T	1	90	23.29	77.2
	↓	2	90	21.18	27.1
	↓	1	270	22.96	69.8
	↓	2	270	22.33	54.7
	---	Hub	---	20.04	0
	T	1	270	23.60	84.9
4	P_S	o	59	24.56	100
	↓	↓	84	↓	↓
	↓	↓	291	↓	↓
	↓	↓	292	↓	↓
	P_T	1	76	23.85	78.2
	↓	2	76	22.25	27.0
	↓	1	295	23.42	65.4
	↓	2	295	22.63	40.2
	↓	3	295	21.82	13.6
4	---	Hub	---	21.41	0
	T	1	295	24.21	88.3
	↓	1	120	24.26	92.8
	↓	2	↓	23.65	73.2
	↓	3	↓	23.01	52.8
	↓	4	↓	22.40	32.2
	↓	5	↓	21.74	10.9
	↓	1	338	24.26	92.8
	↓	2	↓	23.65	73.2
	↓	3	↓	23.01	52.8
	↓	4	↓	22.40	32.2
	↓	5	↓	21.76	10.9
7f	P_T	1	70	46.23	86.2
	↓	2	↓	45.06	65.6
	↓	3	↓	41.40	41.3
	↓	4	↓	40.13	9.8
	T	1	↓	47.35	95.5
	↓	2	↓	45.06	76.3
	↓	3	↓	42.65	54.1
	↓	4	↓	40.11	26.9
	---	ID	---	38.07	0
	---	OD	---	47.90	100
(e)					
7g	P_T	1	70	32.89	86.2
	↓	2	↓	28.52	65.6
	↓	3	↓	23.37	41.3
	↓	4	↓	16.69	9.8
	T	1	↓	34.85	95.5
	↓	2	↓	30.78	76.3
	↓	3	↓	26.09	54.1
	↓	4	↓	20.29	26.9
	---	Hub	---	14.61	0
	---	OD	---	35.79	100

[a]See text for definition of symbols.

[b]Inner annular wall is denoted by i, outer annular wall by o; numbers denote rings.

[e]P_T and T for stations 7f and 7g repeated at 270°.

TABLE II. - ENGINE OPERATING PARAMETERS FOR DISTORTED INLET, CLEAN INLET, AND STALL

[Reynolds number index, $\delta/\omega\sqrt{\theta_2}$, 0.5.]

Inlet condition	Nominal speed of low-speed rotor, N_L, rpm	Corrected speed of low-speed rotor, $N_L/\sqrt{\theta_2}$, rpm	Rotor speed ratio, N_H/N_L	Inlet total pressure distortion, $\frac{P_{T,max} - P_{T,min}}{\bar{P}_{T,r}}$	Inlet flow distortion parameter,[a] KD2
Distorted	7400	7424	1.626	0.057	489
	8600	8644	1.523	.097	847
Clean	7400	7424	1.637	-----	---
	8600	8644	1.522	-----	---
Stall	7400	7349	1.654	0.094	850
	8600	8228	1.451	.131	1180

[a]A Pratt & Whitney-developed distortion parameter consisting of a summation of circumference- and diameter-weighted values of $[(\bar{P}_T - P_{T,min})/\bar{P}_T]_r$; see ref. 7.

TABLE III. - FACE-AVERAGED VALUES OF TOTAL PRESSURE, STATIC PRESSURE, TOTAL TEMPERATURE, AND FLOW VELOCITY

Measurement	Engine instrumentation station										
	2	2.1	2.3	2.3f	2.6	2.6f	3.0	3.12	4.0	7g	7f
Nominal speed of low-speed rotor, N_L, 7400 rpm											
Total pressure, P_T, kN/m^2	50.57	60.85	84.26	70.95	127.48	69.75	169.65	283.10	446.47	64.58	65.33
Static pressure, P_S, kN/m^2	46.26	56.14	76.39	63.39	111.61	63.34	140.55	241.66	414.60	------	------
Total temperature, T, K	295.0	317.2	347.8	337.2	398.9	338.9	442.8	518.3	599.4	631.1	340.0
Flow velocity, V, m/sec	122.04	120.52	138.90	146.85	172.85	------	215.89	214.73	158.89	------	------
Nominal speed of low-speed rotor, N_L, 8600 rpm											
Total pressure, P_T, kN/m^2	49.50	62.98	97.57	386.53	162.56	86.86	233.15	396.48	654.27	85.70	82.80
Static pressure, P_S, kN/m^2	45.95	55.37	82.91	77.84	135.55	80.30	187.19	335.39	625.58	------	------
Total temperature, T,K	296.1	325.0	367.8	363.9	437.8	364.4	496.1	580.0	683.3	779.4	367.8
Flow velocity, V, m/sec	111.80	116.71	184.07	143.96	211.17	------	246.43	233.45	131.73	------	------

TABLE IV. - CALCULATED ENGINE PERFORMANCE PARAMETERS FOR DISTORTED AND CLEAN INLETS

Inlet condition	Nominal speed of low-speed rotor, N_L, rpm	Corrected inlet airflow, $W_{a,2}\sqrt{\theta_2}/\delta_2$, kg/sec	Bypass ratio, $W_{a,F}/W_{a,C}$	Engine pressure ratio, $P_{T,7}/P_{T,2}$	Engine temperature ratio, T_7/T_2	Core stream efficiency, η_C	Fan stream efficiency, η_F
Distorted	7400	81.4	1.371	1.299	1.549	82.7	72.4
	8600	97.7	.952	1.698	1.871	80.3	74.1
Clean	7400	82.0	1.267	1.305	1.599	82.4	72.9
	8600	96.8	.980	1.695	1.932	81.7	72.8

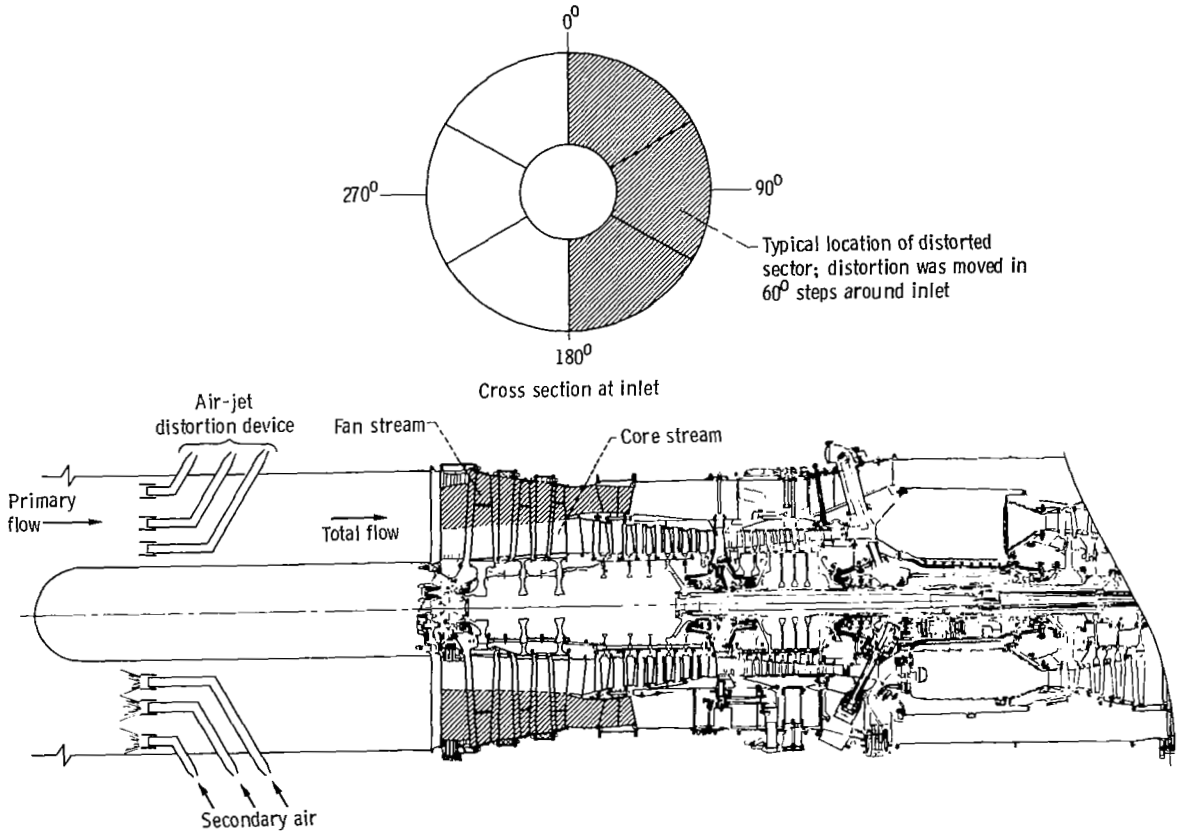

Figure 1. - Facility inlet and engine compression system.

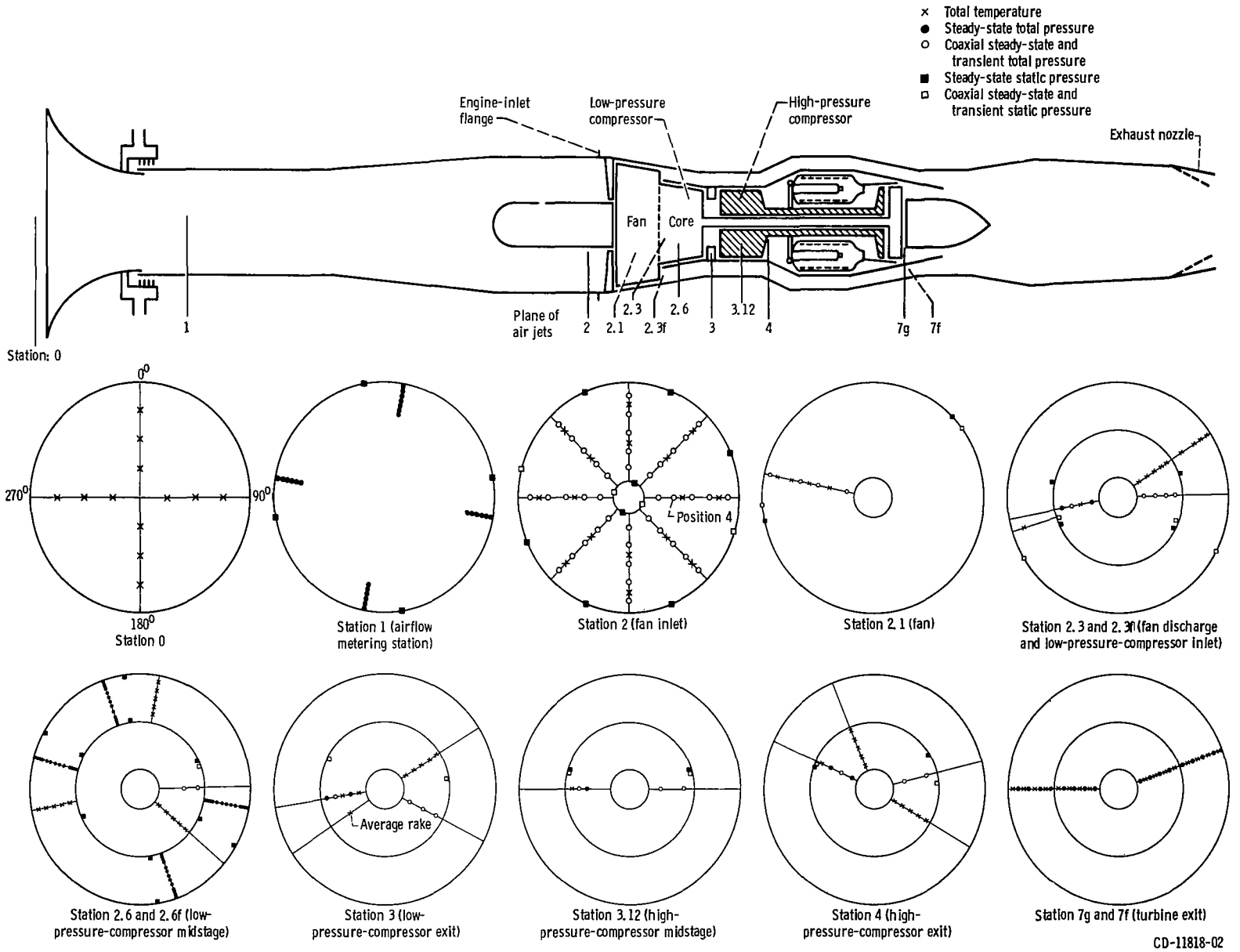

Figure 2. - Instrumentation layout for TF30-P-3 turbofan engine. (Instrumentation stations viewed looking upstream.)

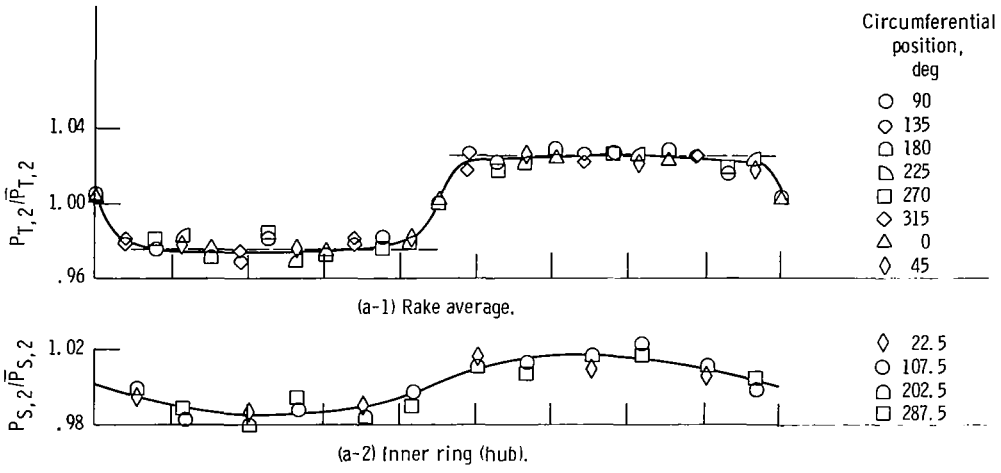

(a) Nominal low-speed-rotor speed, 7400 rpm.

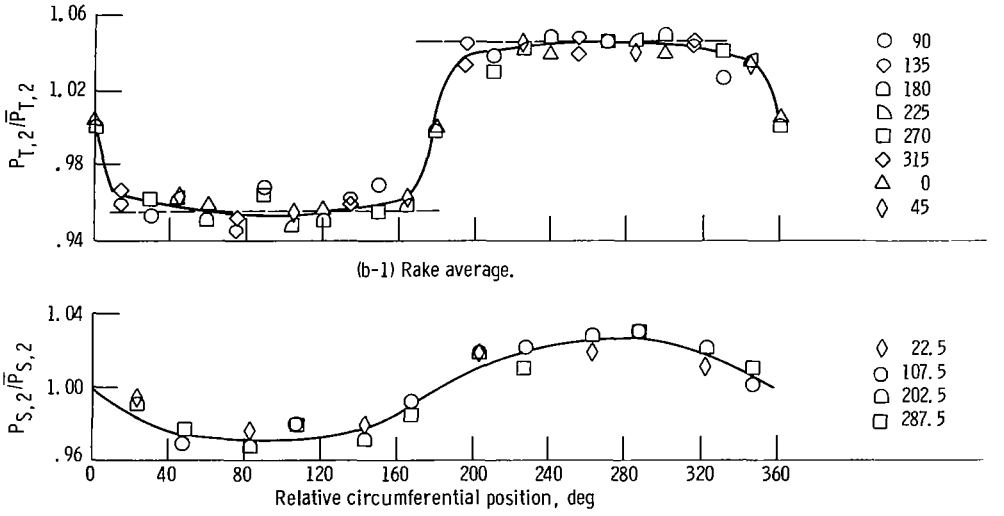

(b) Nominal low-speed-rotor speed, 8600 rpm.

Figure 3. - Total and static pressure distortion patterns measured at engine inlet (station 2).

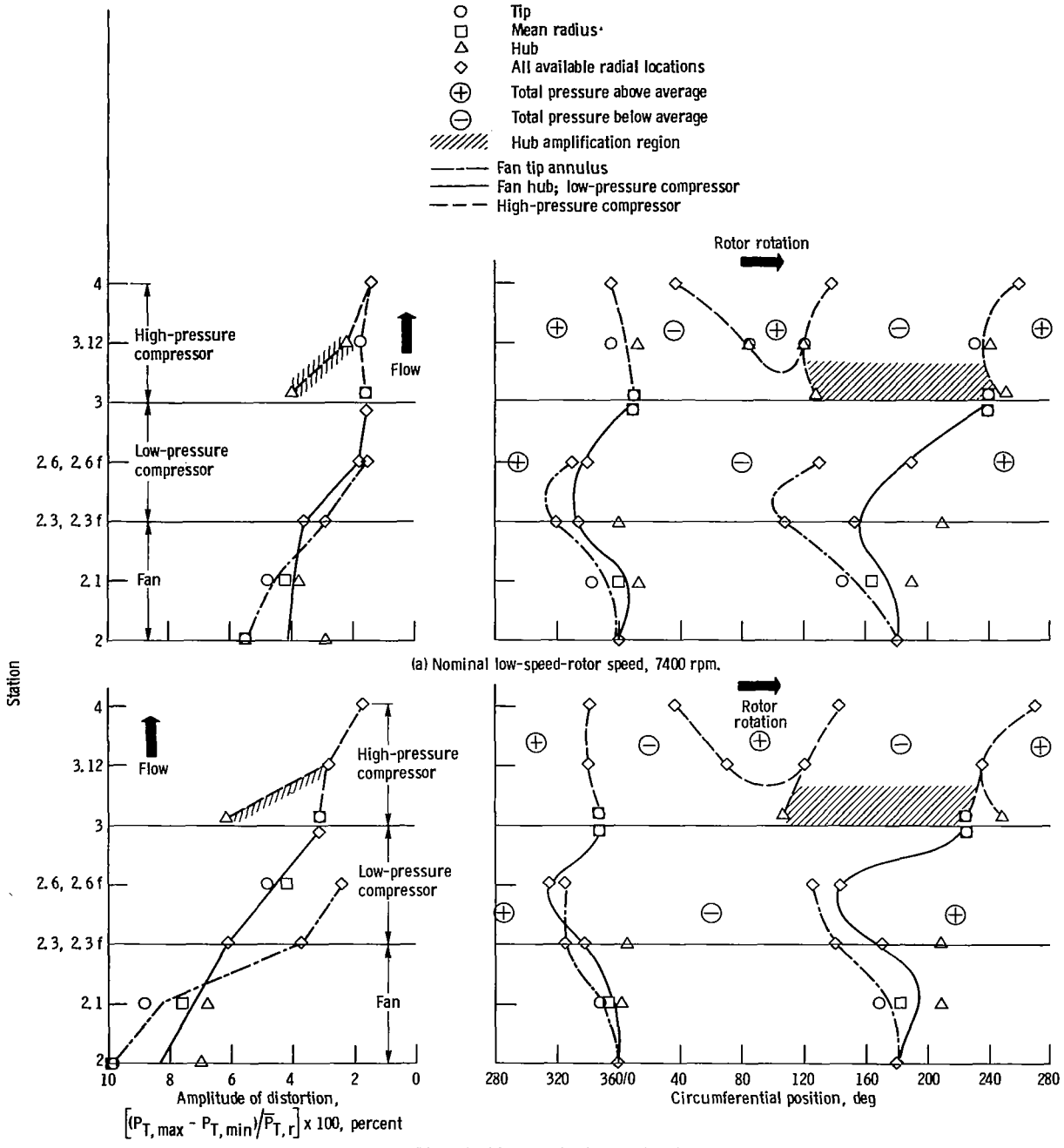

(a) Nominal low-speed-rotor speed, 7400 rpm.

(b) Nominal low-speed-rotor speed, 8600 rpm.

Figure 4. - Total pressure distortion - axial variation in amplitude and circumferential position.

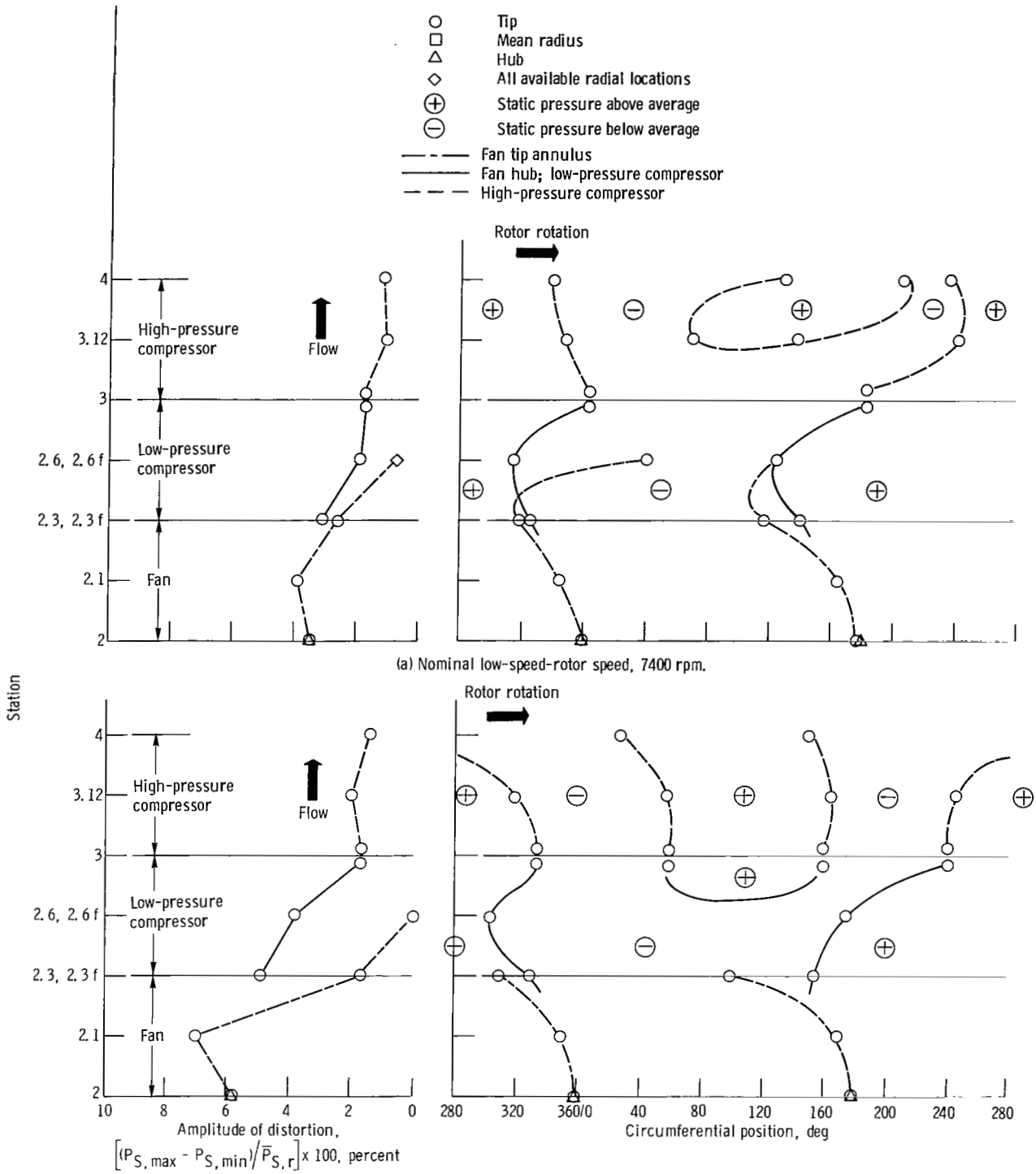

(a) Nominal low-speed-rotor speed, 7400 rpm.

(b) Nominal low-speed-rotor speed, 8600 rpm.

Figure 5. - Static pressure distortion - axial variation in amplitude and circumferential position.

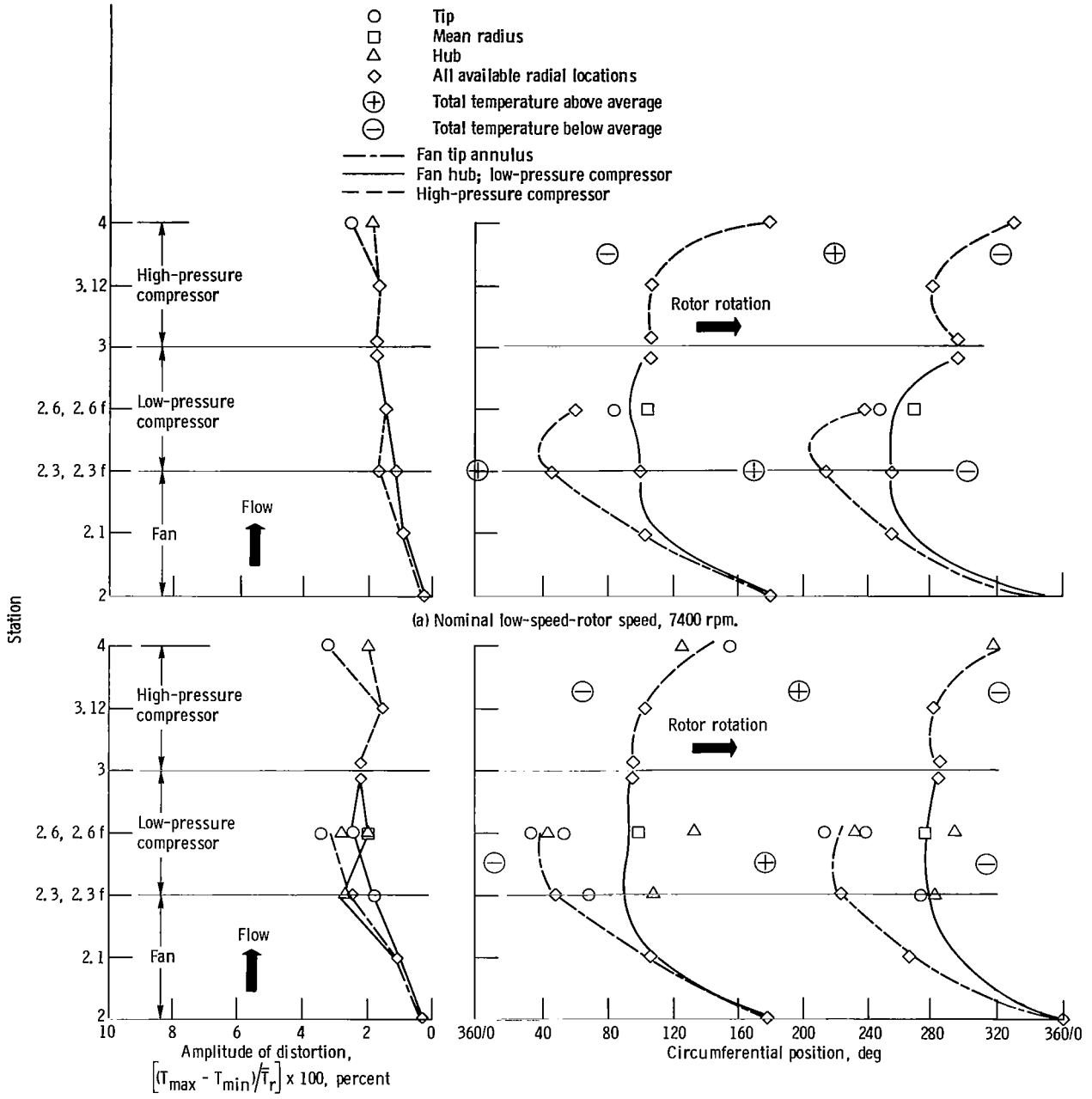

(a) Nominal low-speed-rotor speed, 7400 rpm.

(b) Nominal low-speed-rotor speed, 8600 rpm.

Figure 6. - Temperature distortion - axial variation in amplitude and circumferential position.

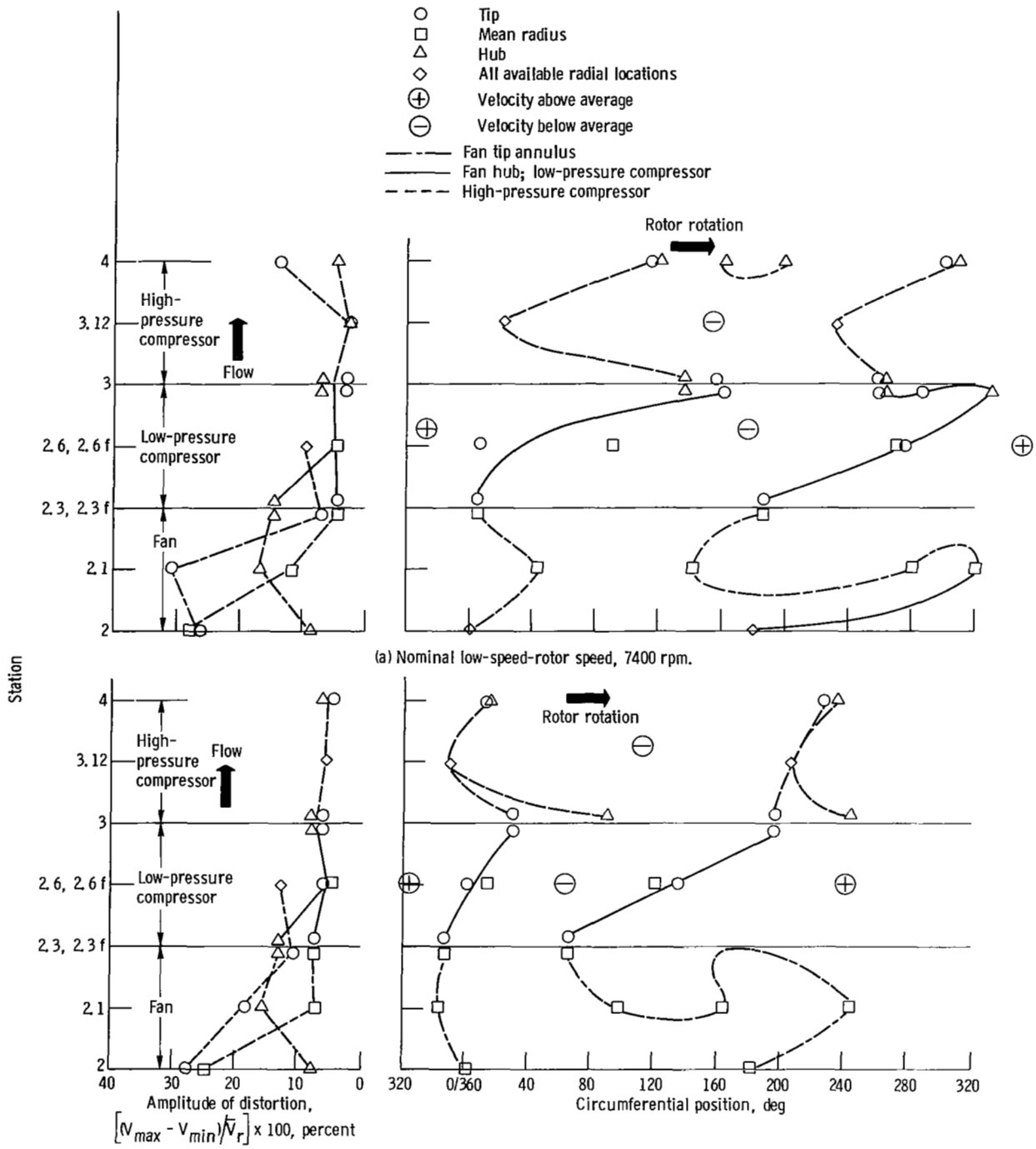

(a) Nominal low-speed-rotor speed, 7400 rpm.

(b) Nominal low-speed-rotor speed, 8600 rpm.

Figure 7. - Flow velocity distortion - axial variation in amplitude and circumferential position.

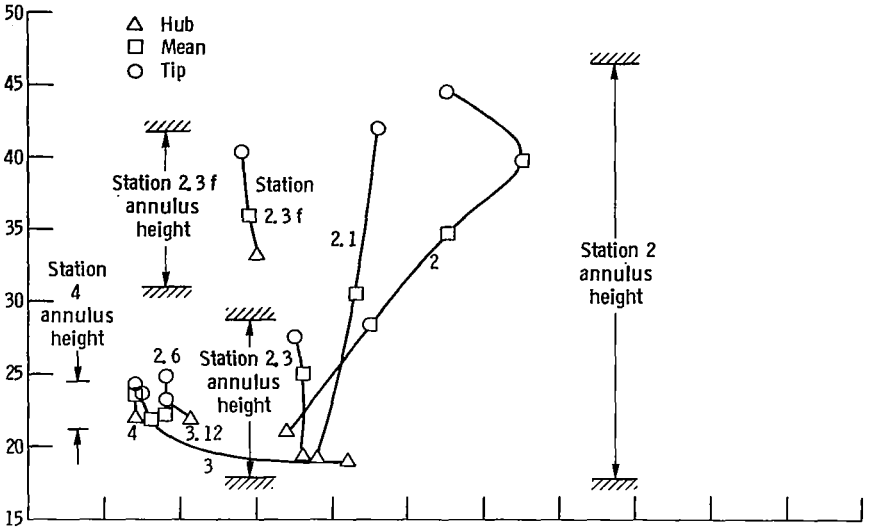

(a) Nominal low-speed-rotor speed, 7400 rpm.

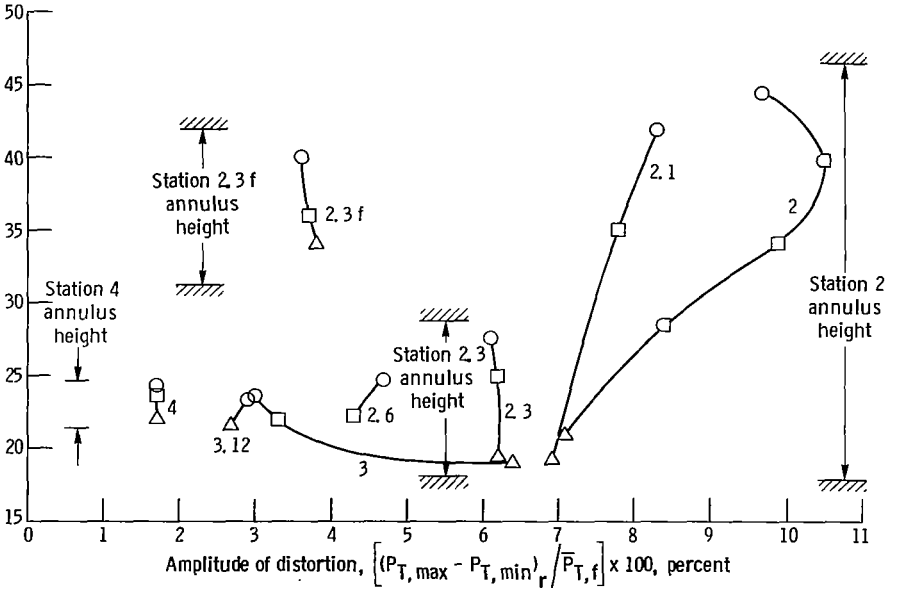

(b) Nominal low-speed-rotor speed, 8600 rpm.

Figure 8. - Total pressure distortion - radial variation.

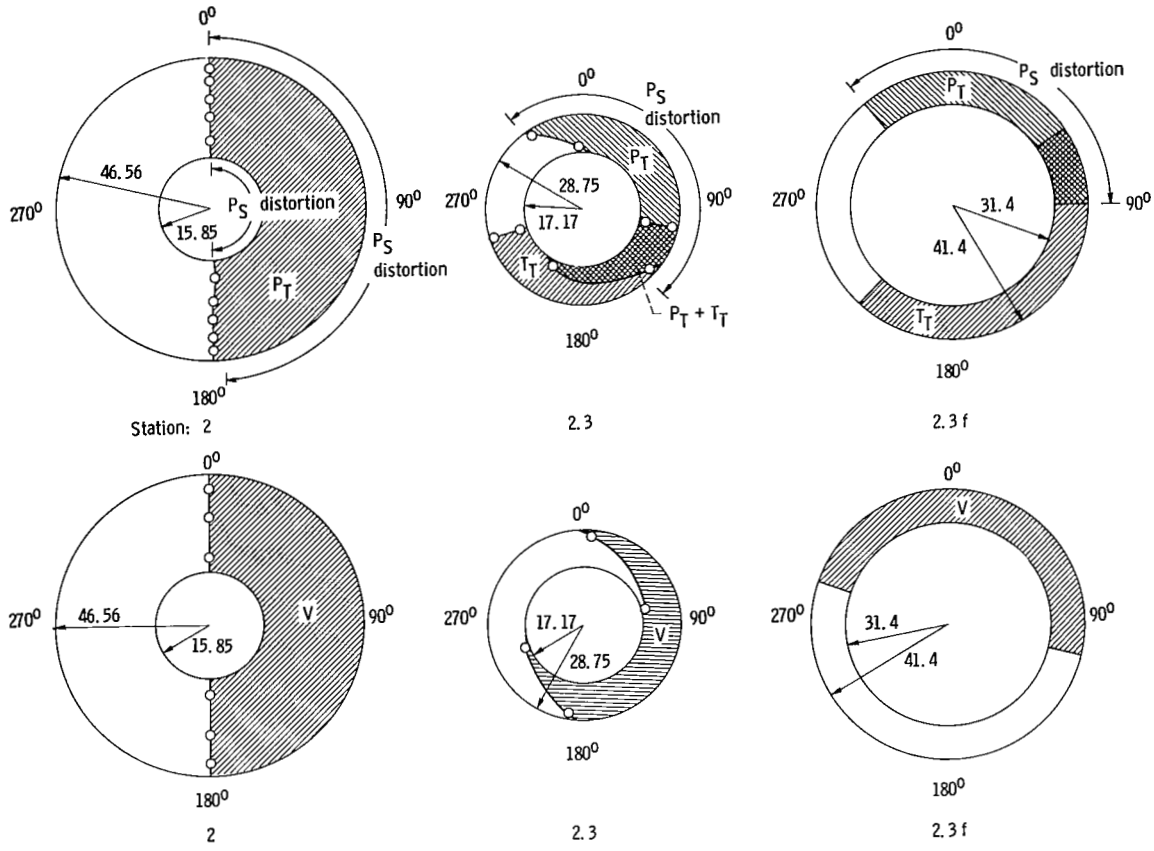

(a) Nominal low-speed-

Figure 9. - Radial and circumferential extend of distorted

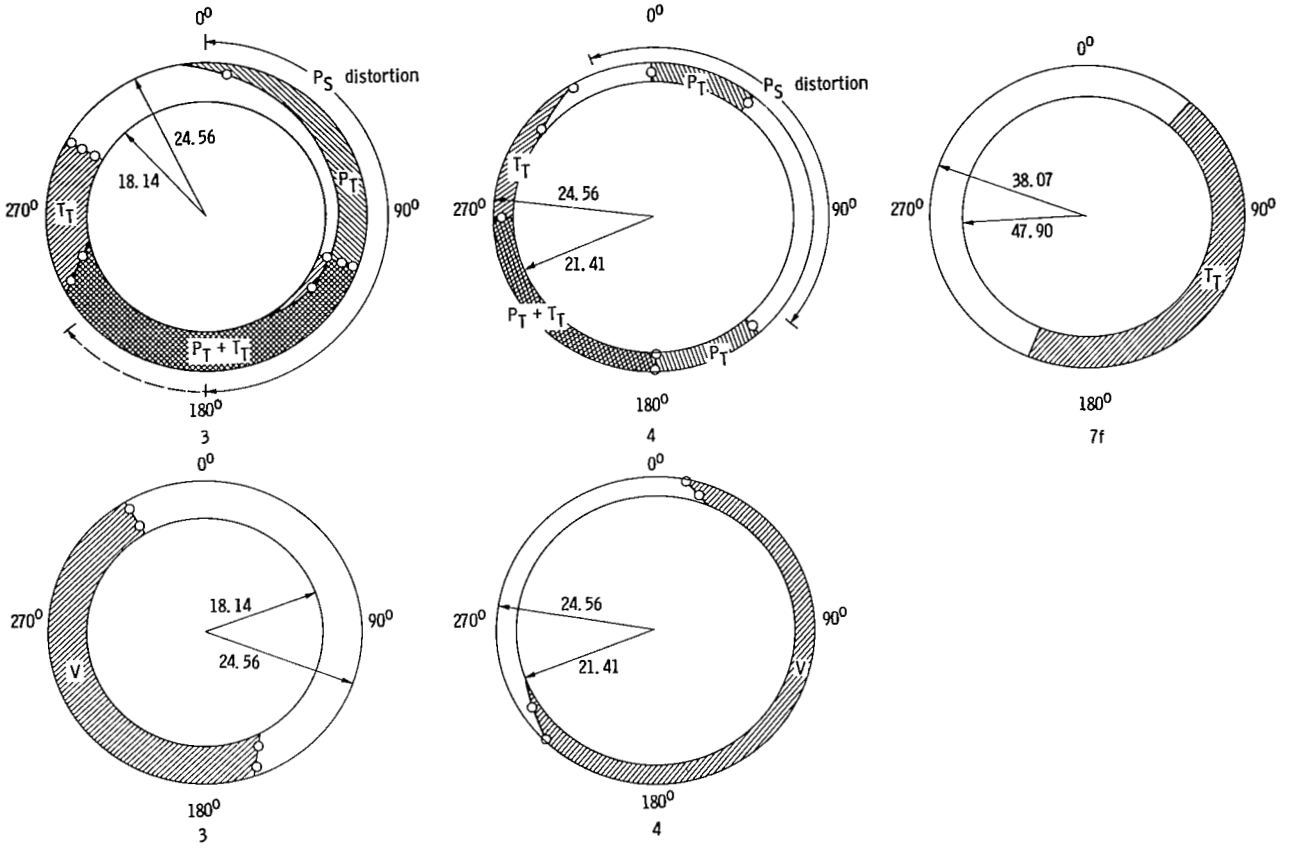

rotor speed, 7400 rpm.

sectors, looking upstream (clockwise rotor rotation).

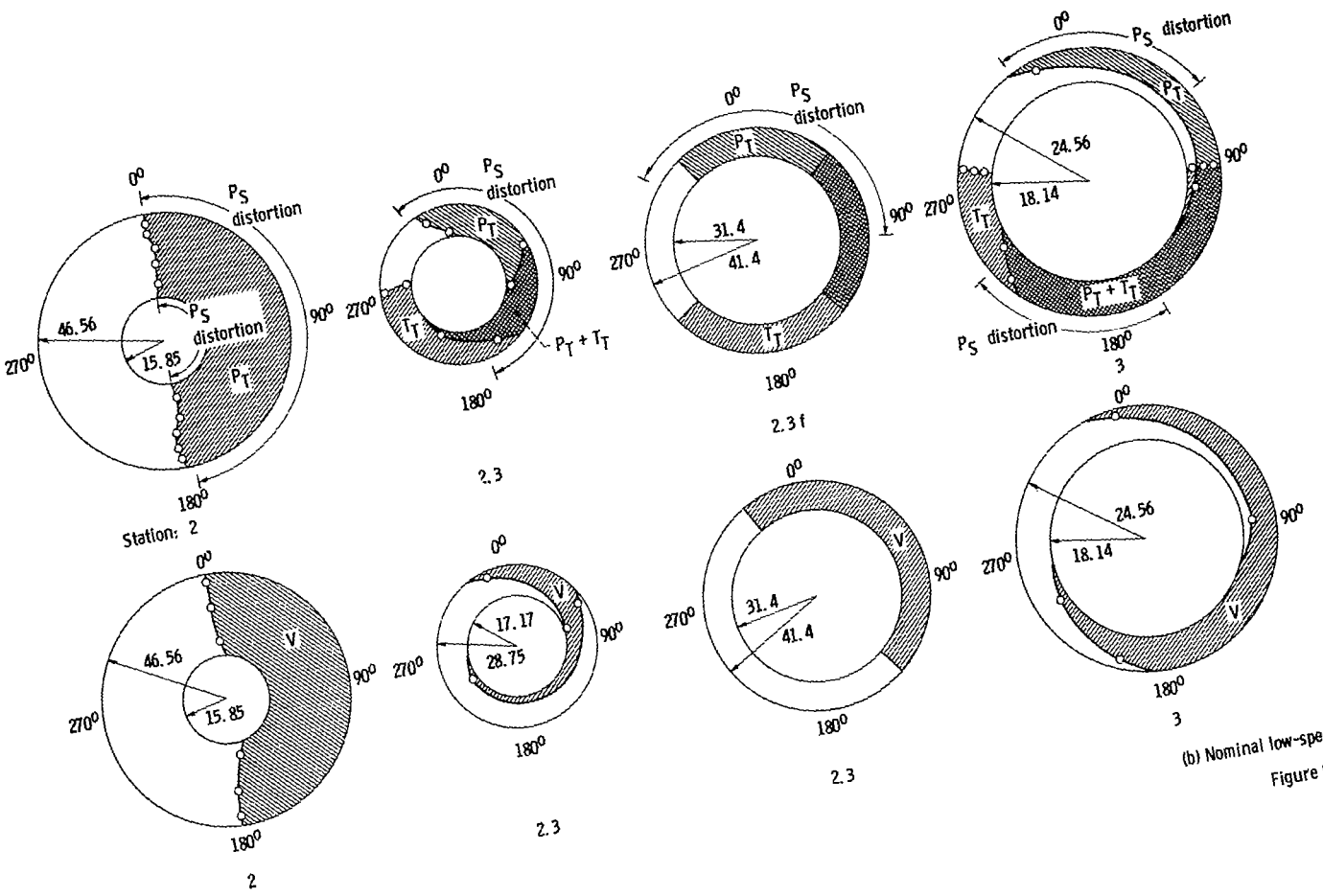

(b) Nominal low-speed-

Figure 9. -

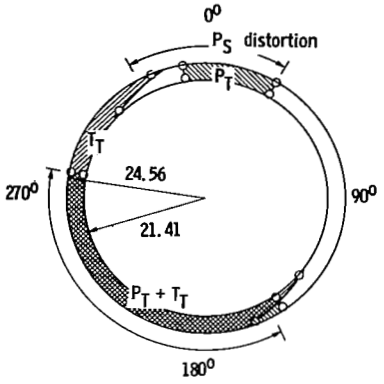

4

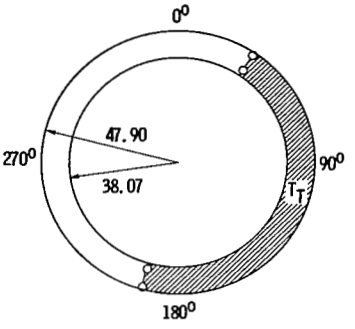

7f

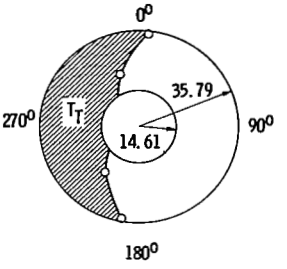

7g

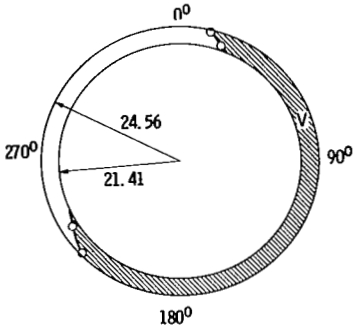

4

rotor speed, 8600 rpm.

Concluded.

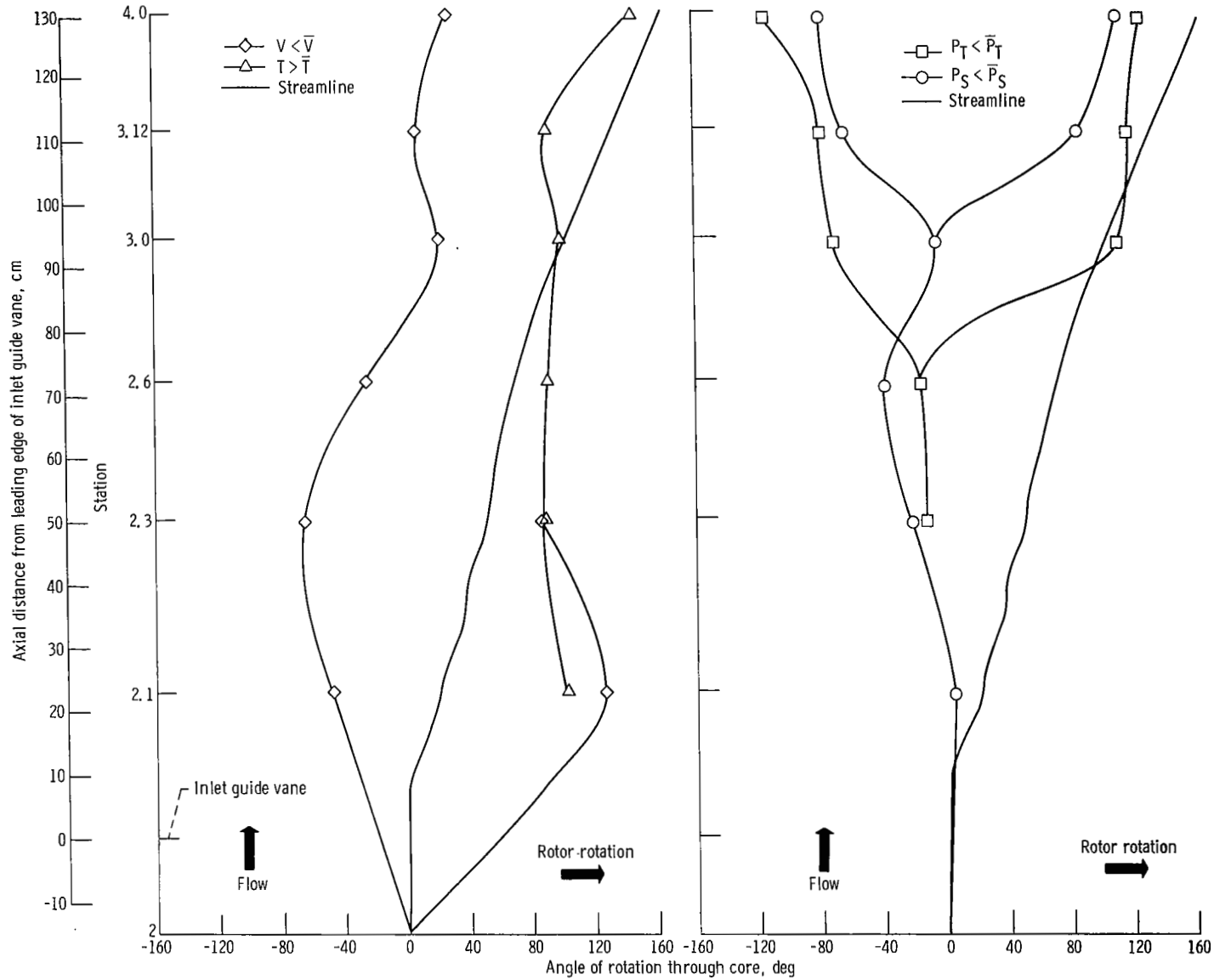

(a) Total temperature and flow velocity.

(b) Total and static pressure.

Figure 10. - Distorted-area centerlines in core compared to calculated streamline. Nominal low-speed-rotor speed, 8600 rpm.

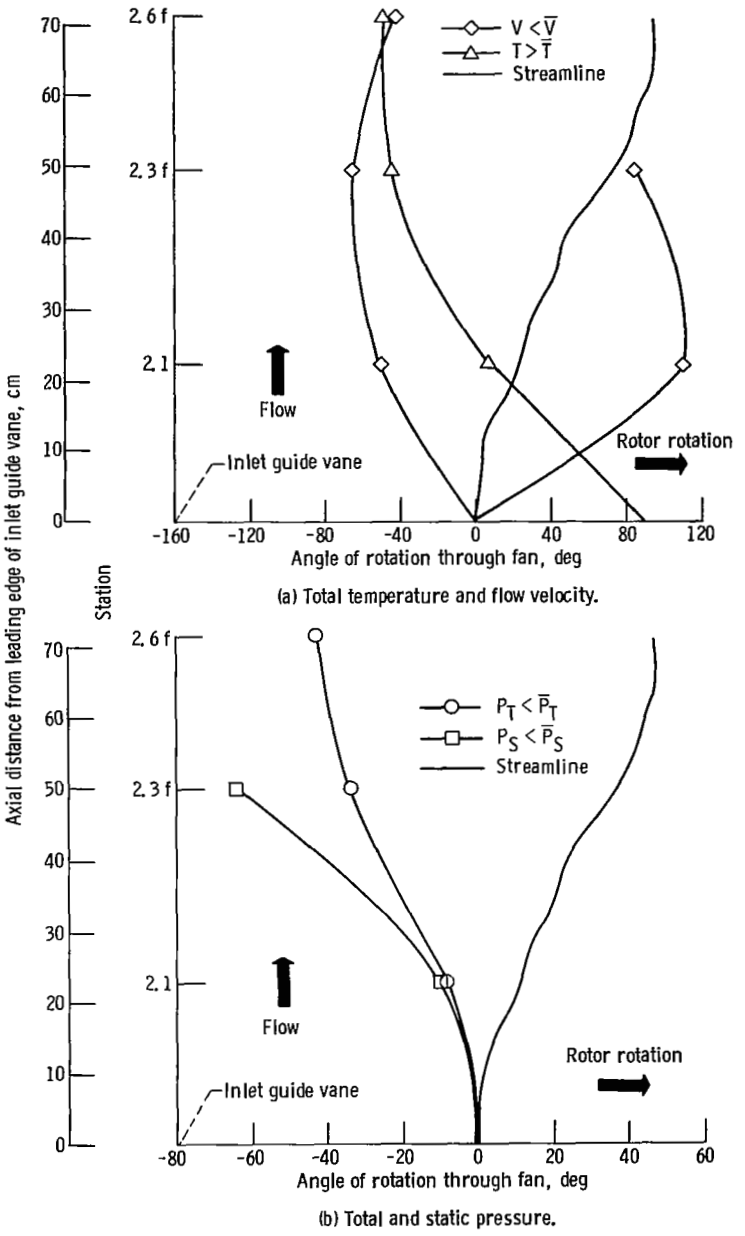

Figure 11. - Distorted-area centerlines in fan compared to calculated streamline. Nominal low-speed-rotor speed, 8600 rpm.

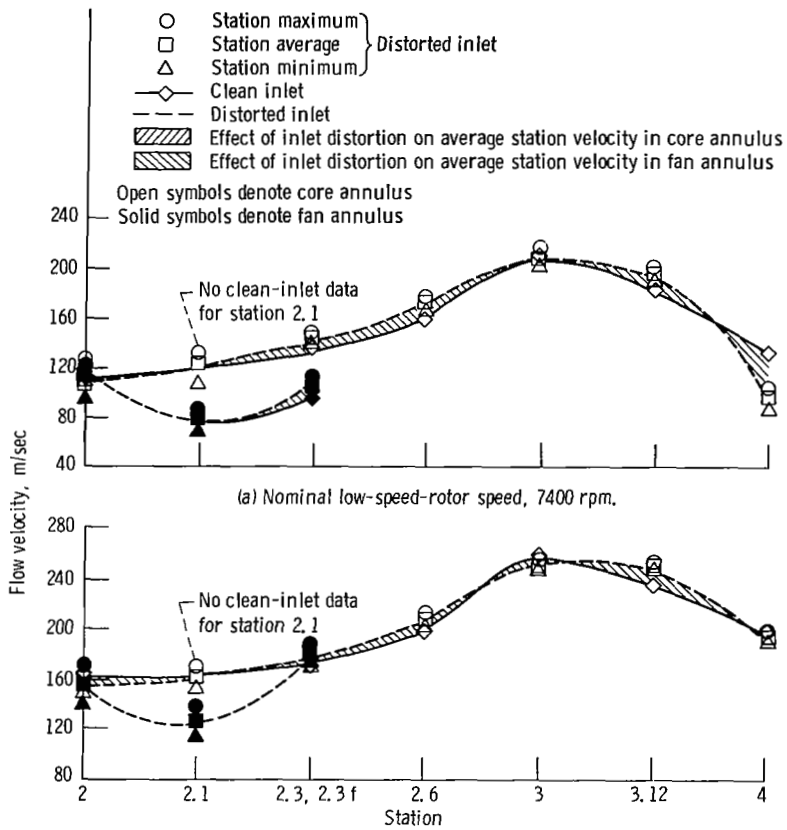

(a) Nominal low-speed-rotor speed, 7400 rpm.

(b) Nominal low-speed-rotor speed, 8600 rpm.

Figure 12. - Effect of inlet distortion on average flow velocity.

APPENDIX - CIRCUMFERENTIAL VARIATION IN TOTAL PRESSURE, STATIC PRESSURE, TOTAL TEMPERATURE, FLOW VELOCITY, AND MACH NUMBER FOR PROBE AND RAKE DATA

All the data used to determine the flow conditions within the engine when it was operated with inlet distortion are presented in figures 13 to 18. When ring numbers are given, they are equivalent to the position numbers given in table I. The data are shown as probe values or rake average values plotted against relative circumferential position. All probe and rake average values have been normalized to their average for the six distortion runs made at each of the two speeds. The data are given in the following conditions:

(1) Raw data values of total and static pressure have been corrected for run-to-run deviations of the undistorted total pressure at station 2 from the nominal input value of 51 711 N/m^2 (7.5 psi).

(2) Total temperature has been corrected for ram recovery by using a straight-line approximation of the unshielded-wedge curve from reference 6.

(3) Flow velocity and Mach number have been calculated based on tip static pressures everywhere except stations 2, 2.3f, and 2.6f.

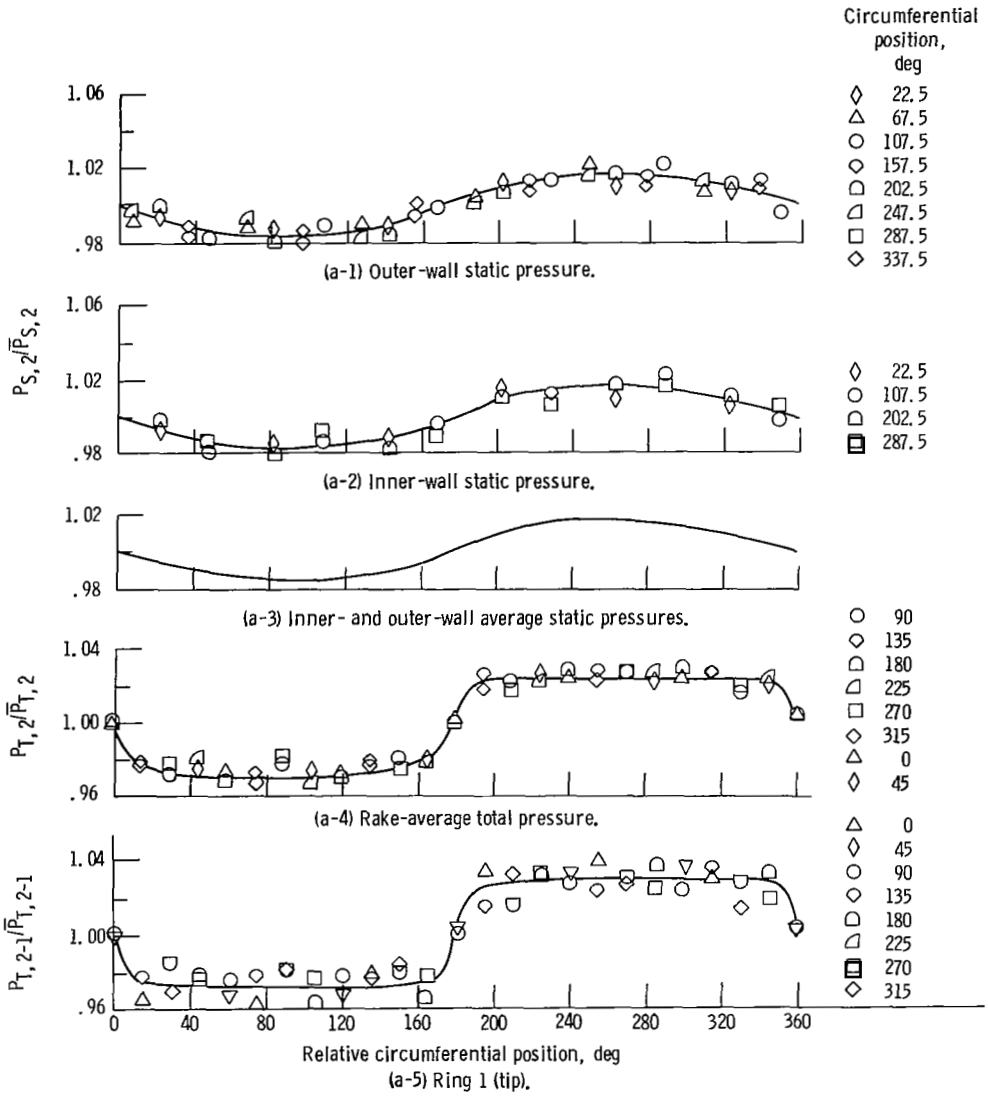

(a) Static and total pressures at station 2.

Figure 13. - Circumferential variation in total and static pressure for nominal low-speed-rotor speed of 7400 rpm.

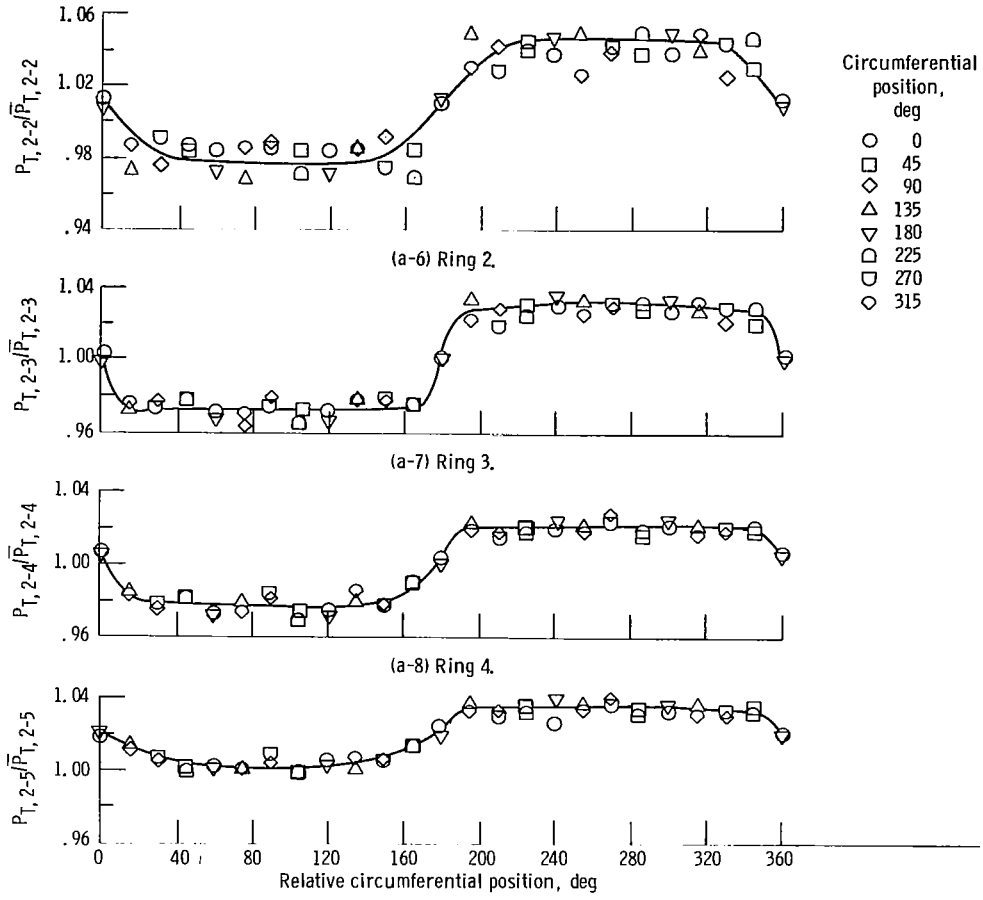

(a-6) Ring 2.

(a-7) Ring 3.

(a-8) Ring 4.

(a-9) Ring 5 (hub).

(a) Concluded.

Figure 13. - Continued.

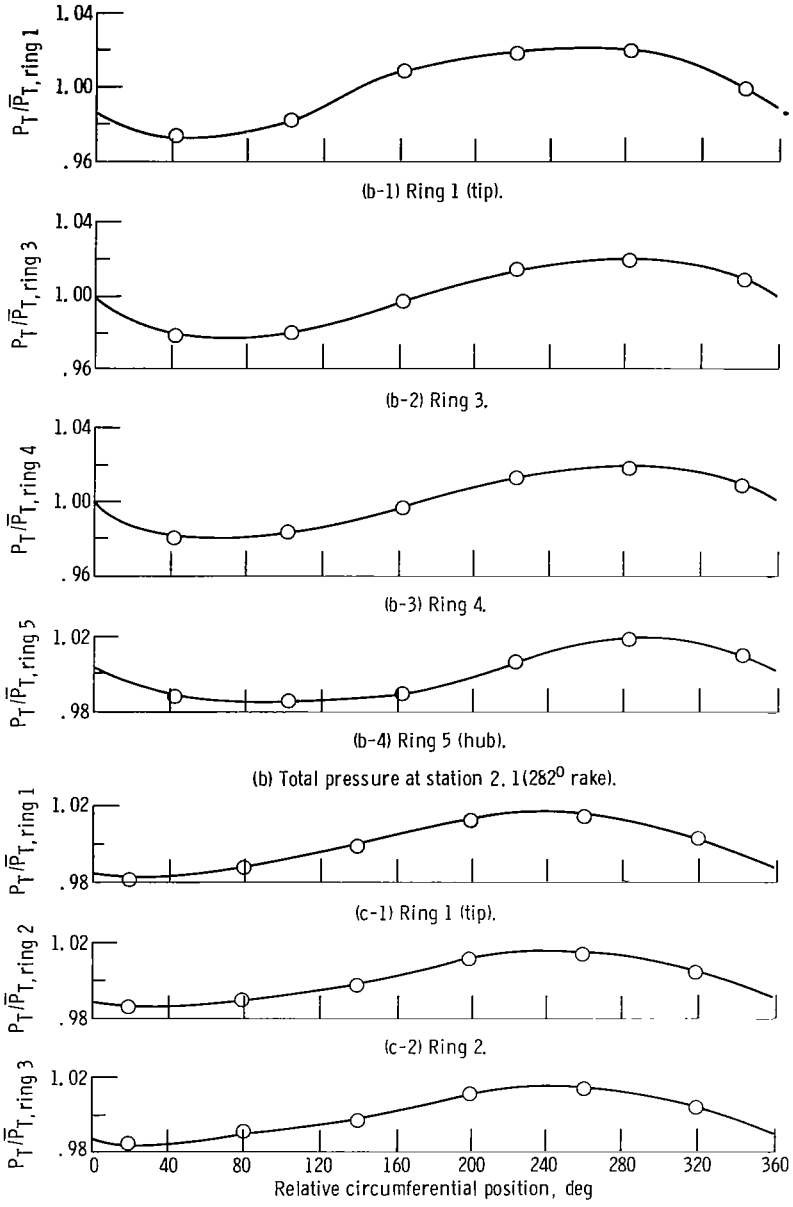

Figure 13. - Continued.

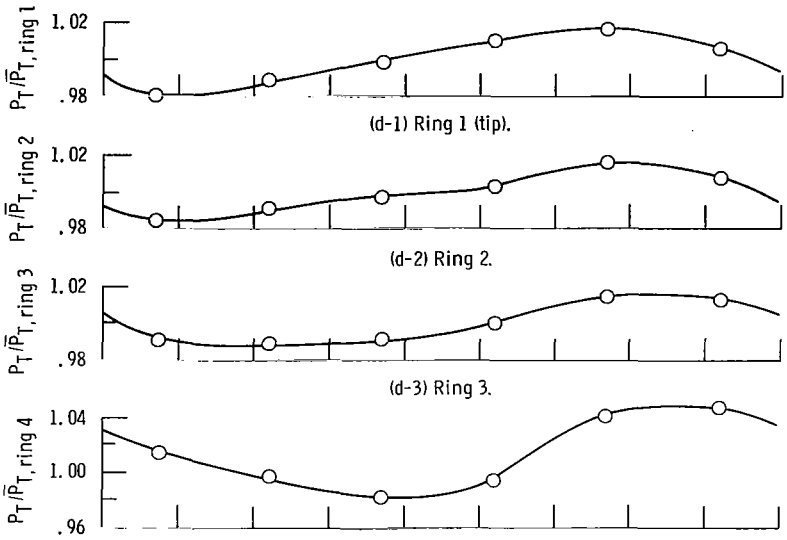

(d-1) Ring 1 (tip).

(d-2) Ring 2.

(d-3) Ring 3.

(d-4) Ring 4 (hub).

(d) Total pressure at station 2.3 (88^0 rake).

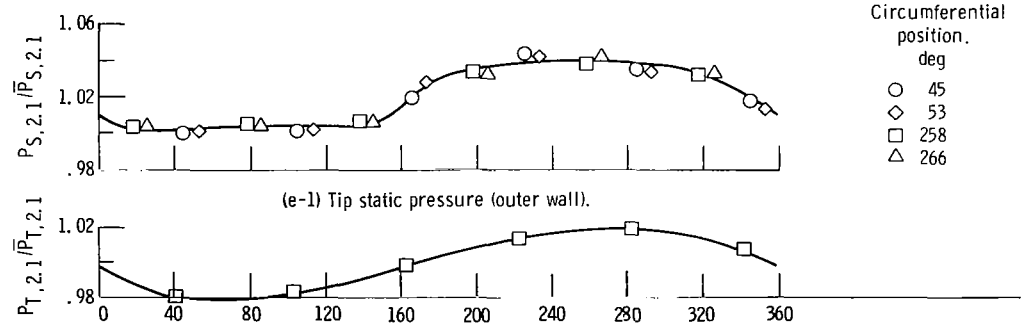

(e-1) Tip static pressure (outer wall).

(e-2) Rake-average total pressure (282^0 rake).

(e) Static and total pressures at station 2.1.

Figure 13. - Continued.

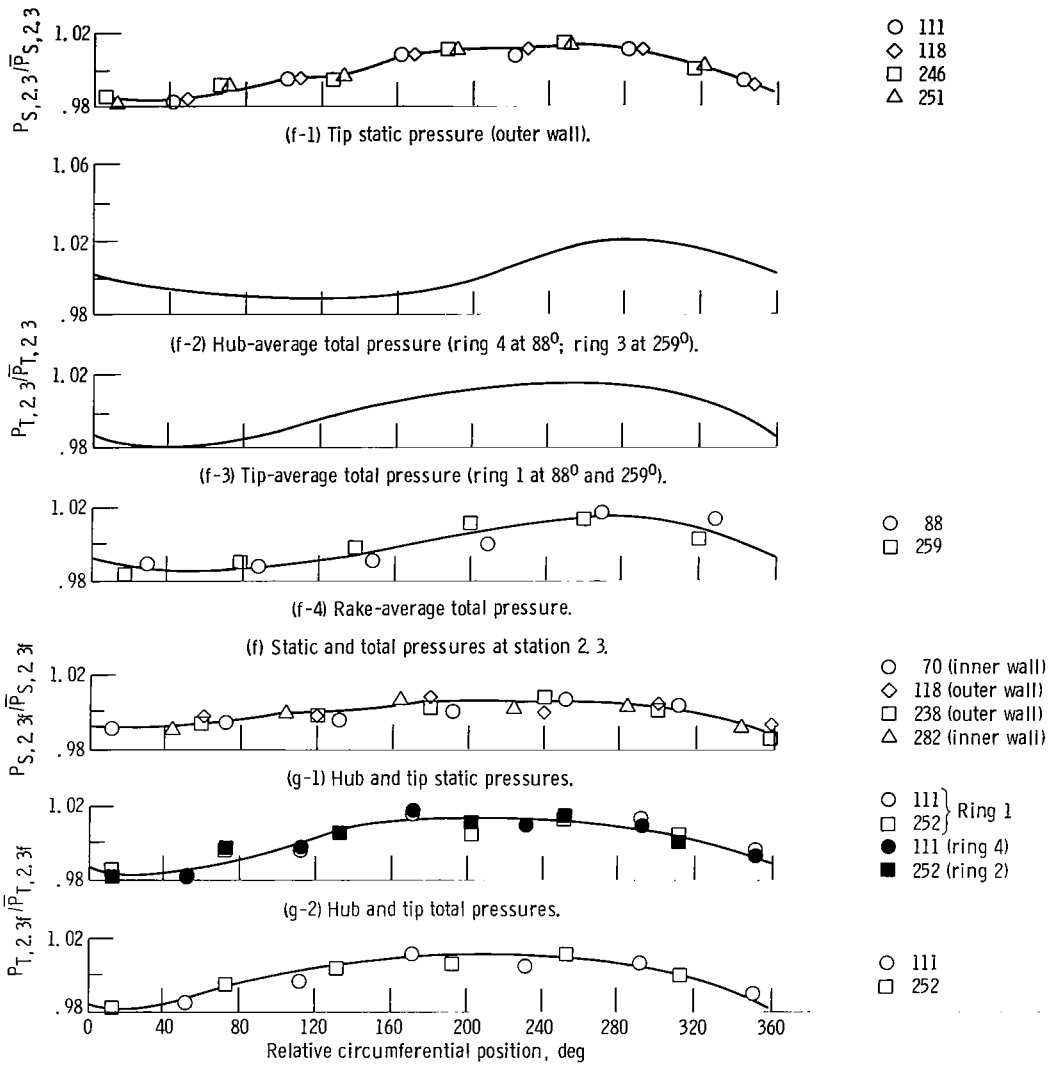

Figure 13. - Continued.

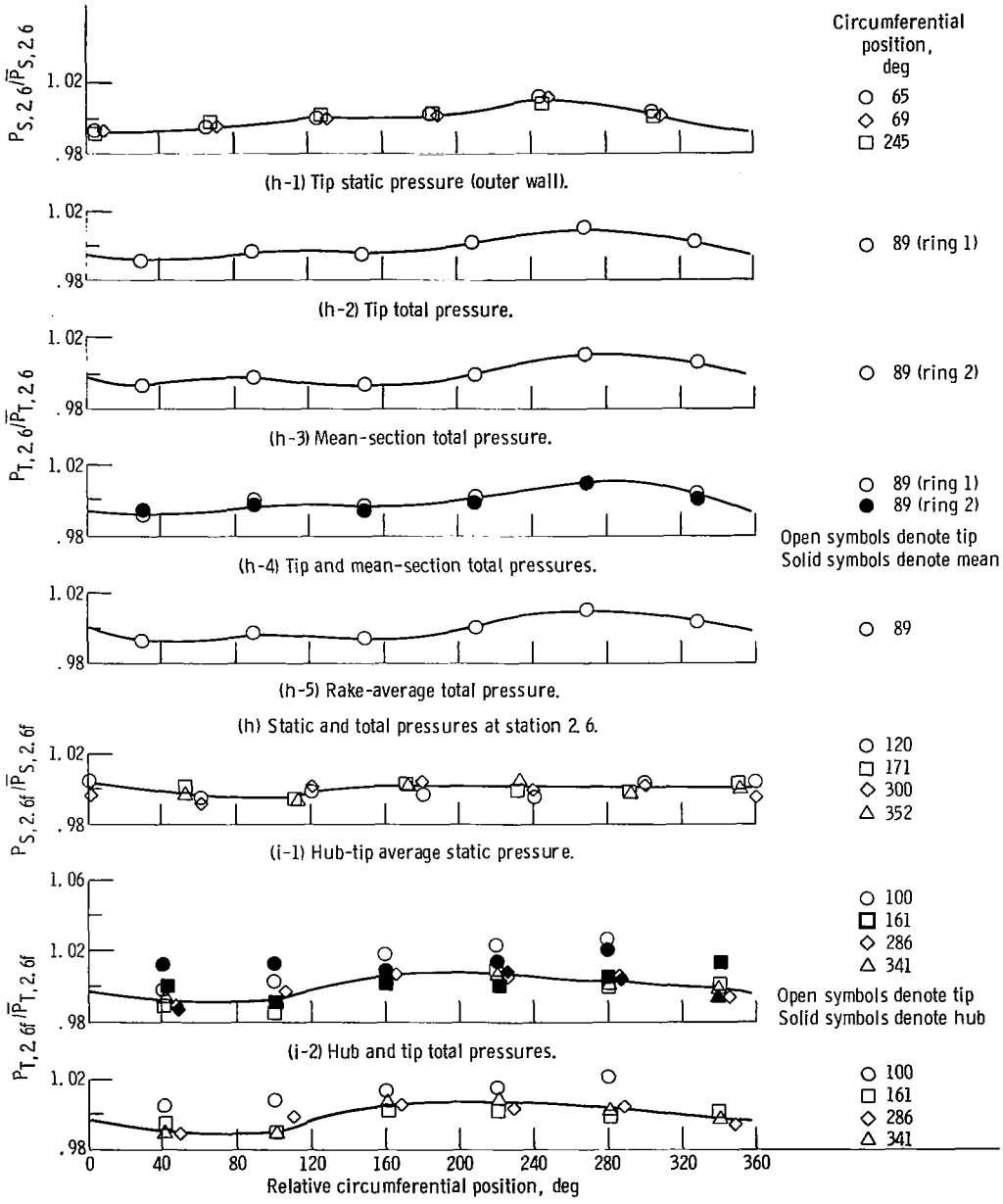

(h-1) Tip static pressure (outer wall).

(h-2) Tip total pressure.

(h-3) Mean-section total pressure.

(h-4) Tip and mean-section total pressures.

(h-5) Rake-average total pressure.

(h) Static and total pressures at station 2.6.

(i-1) Hub-tip average static pressure.

(i-2) Hub and tip total pressures.

(i-3) Rake-average total pressure.

(i) Static and total pressures at static 2.6f.

Figure 13. - Continued.

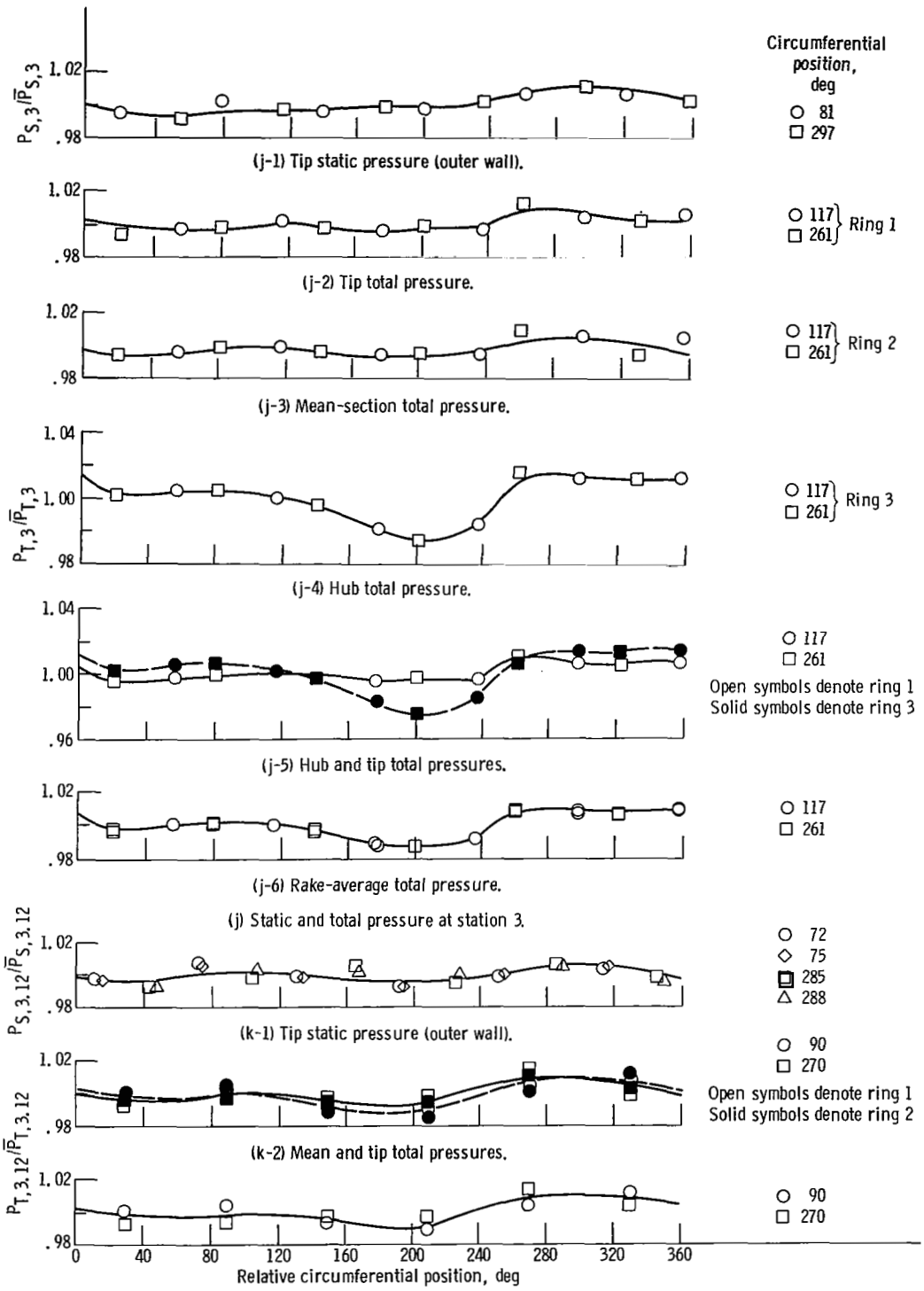

(j-1) Tip static pressure (outer wall).

(j-2) Tip total pressure.

(j-3) Mean-section total pressure.

(j-4) Hub total pressure.

(j-5) Hub and tip total pressures.

(j-6) Rake-average total pressure.

(j) Static and total pressure at station 3.

(k-1) Tip static pressure (outer wall).

(k-2) Mean and tip total pressures.

(k-3) Rake-average total pressure.

(k) Static and total pressures at station 3.12.

Figure 13. - Continued.

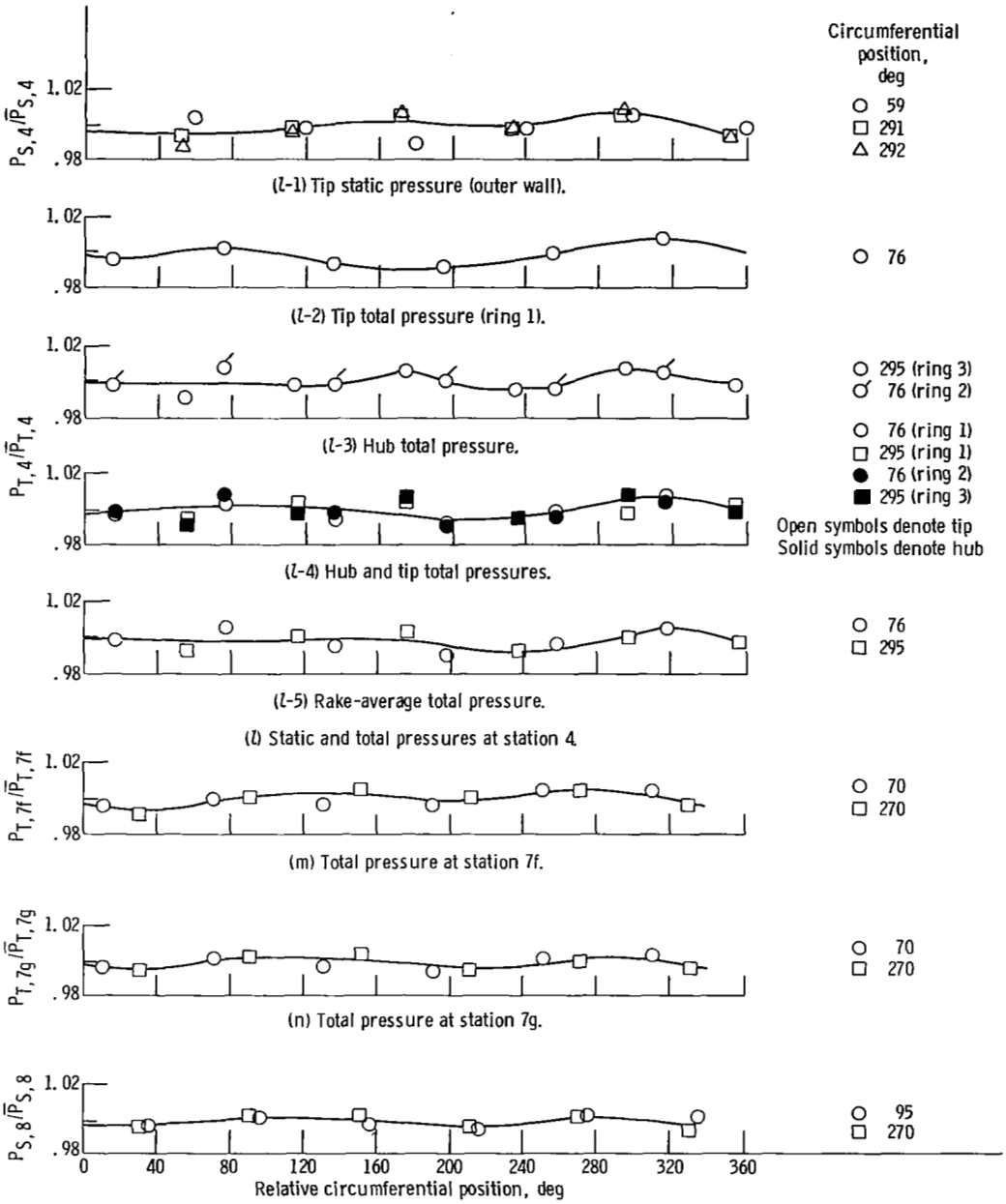

(*l*-1) Tip static pressure (outer wall).

(*l*-2) Tip total pressure (ring 1).

(*l*-3) Hub total pressure.

(*l*-4) Hub and tip total pressures.

(*l*-5) Rake-average total pressure.

(*l*) Static and total pressures at station 4.

(m) Total pressure at station 7f.

(n) Total pressure at station 7g.

(o) Static pressure at station 8.

Figure 13. - Concluded.

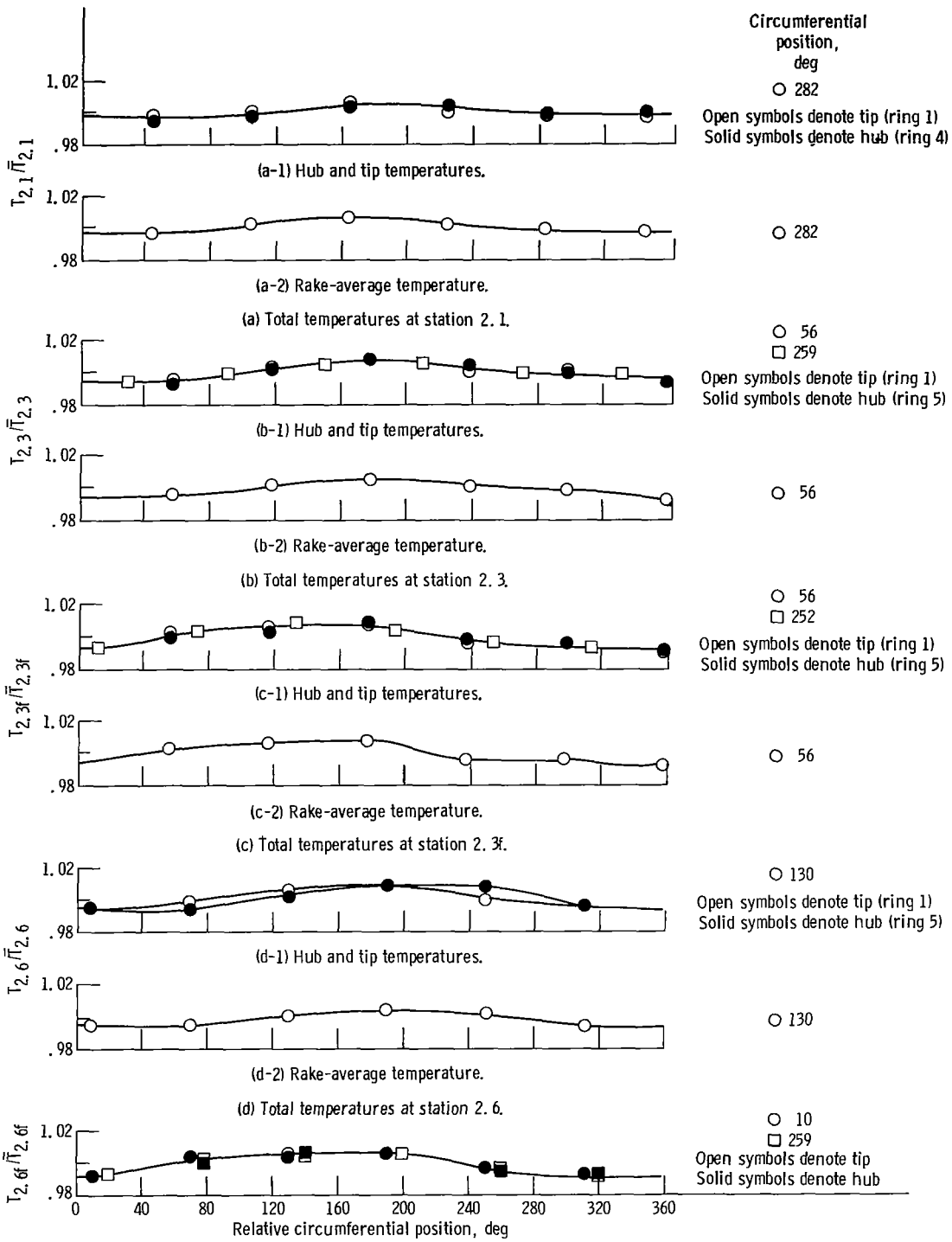

Figure 14. - Circumferential variation in total temperature for nominal low-speed-rotor speed of 7400 rpm.

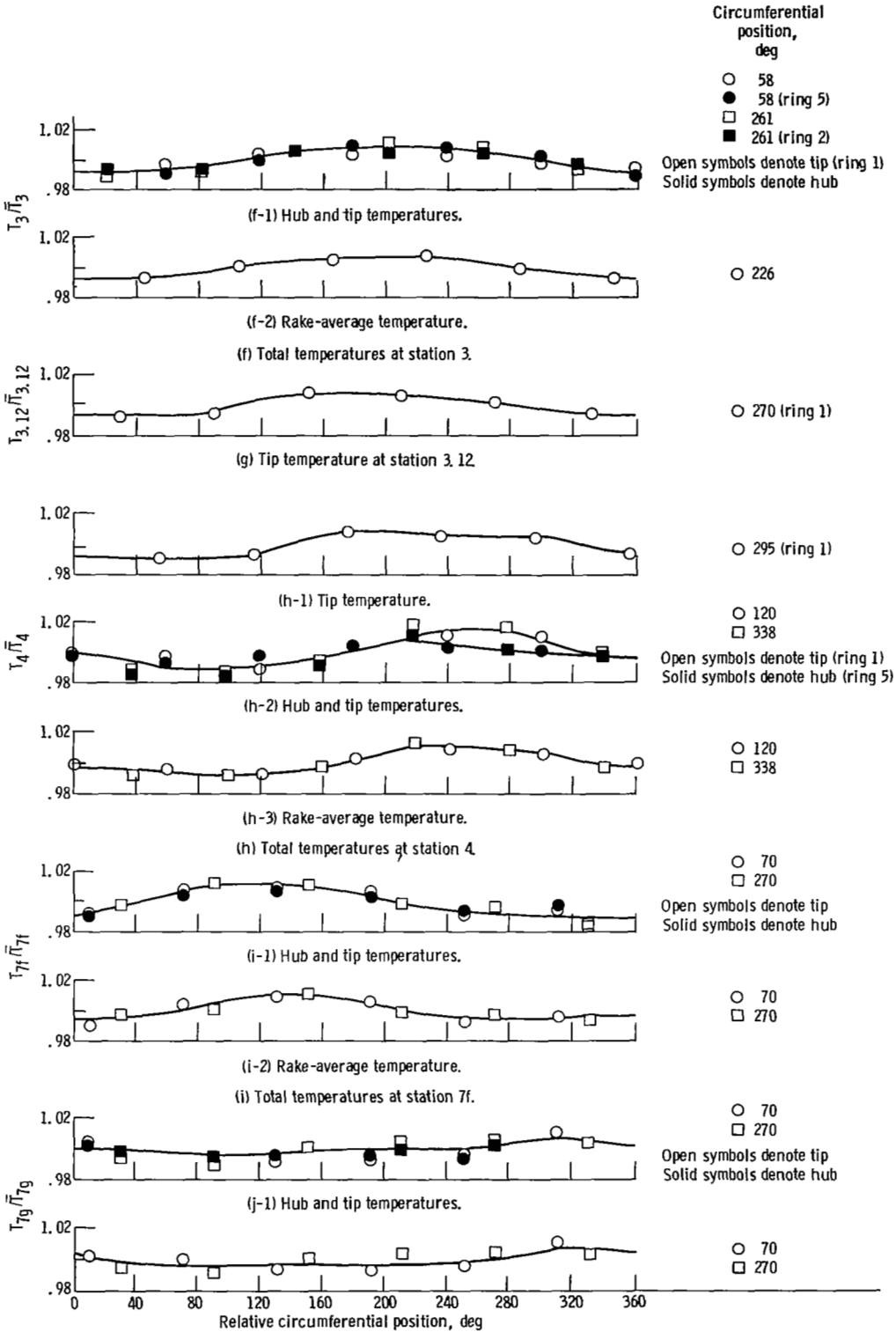

Figure 14. - Concluded.

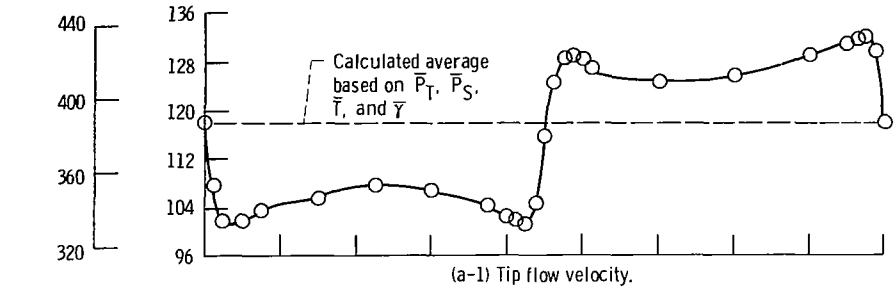

(a-1) Tip flow velocity.

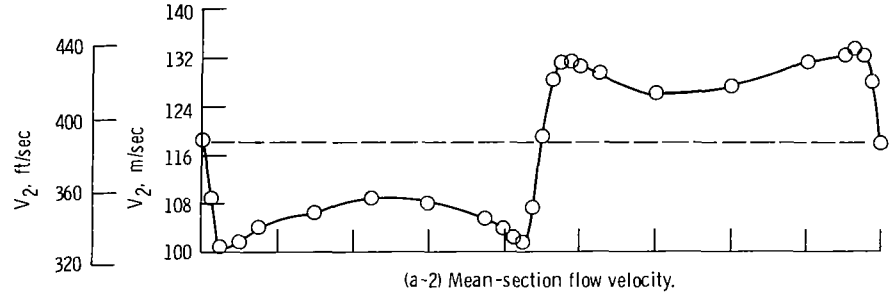

(a-2) Mean-section flow velocity.

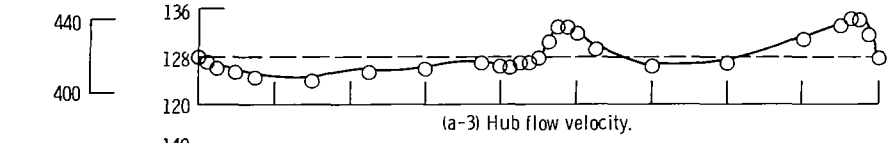

(a-3) Hub flow velocity.

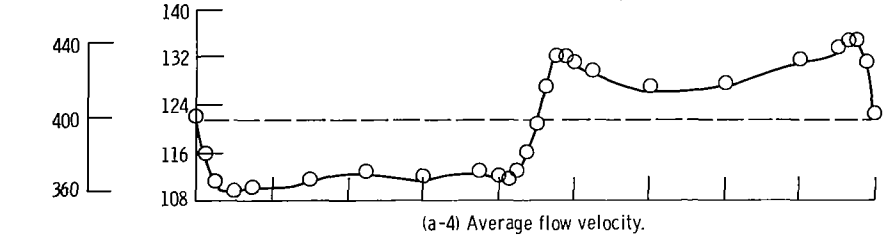

(a-4) Average flow velocity.

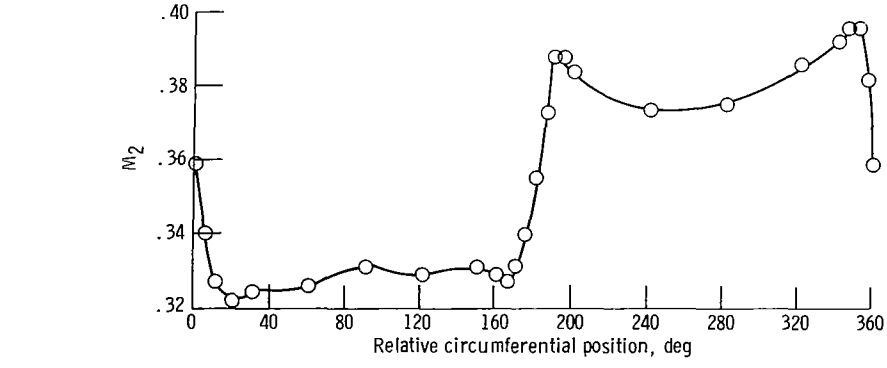

(a-5) Average Mach number.

(a) Station 2.

Figure 15. - Calculated circumferential variation in flow velocity and Mach number for nominal low-speed-rotor speed of 7400 rpm.

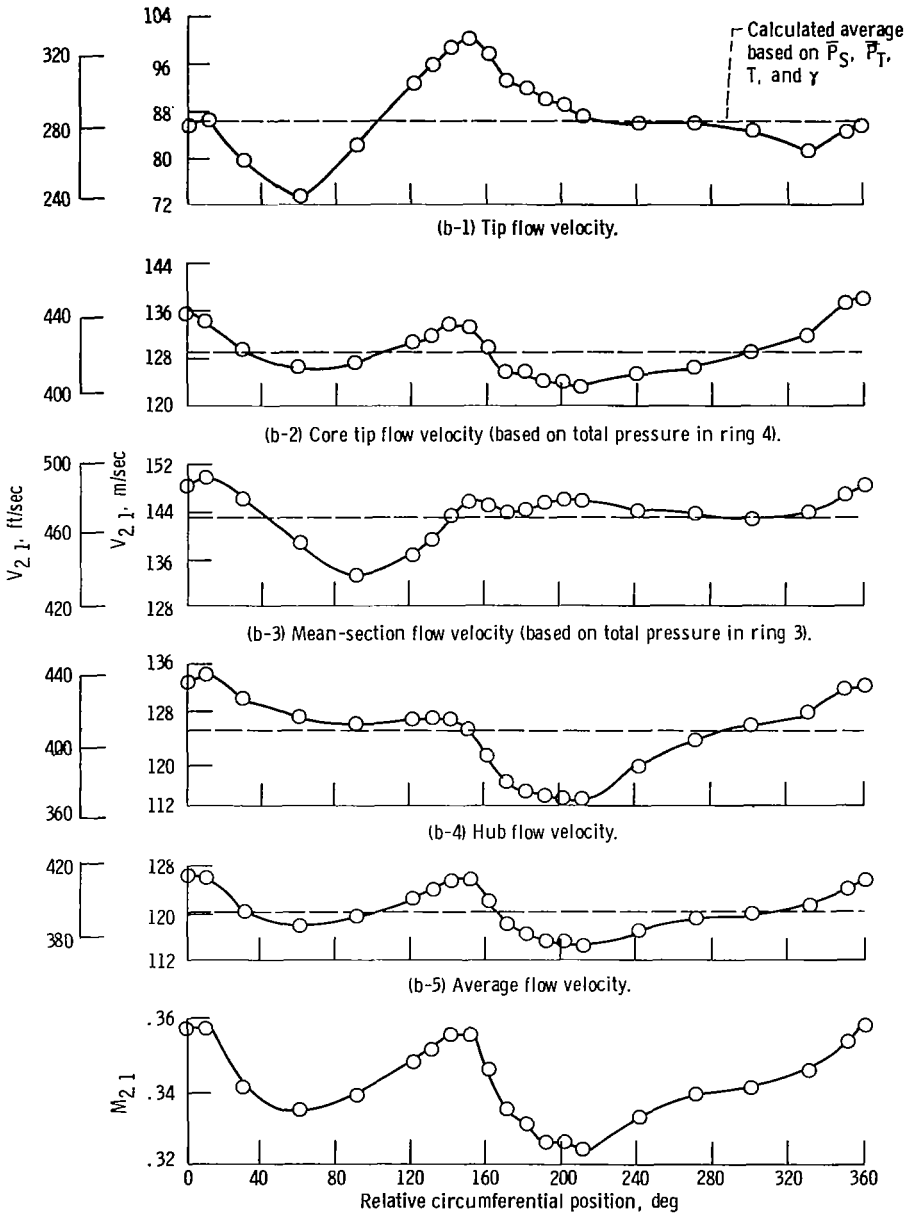

(b) Station 2.1.

Figure 15. - Continued.

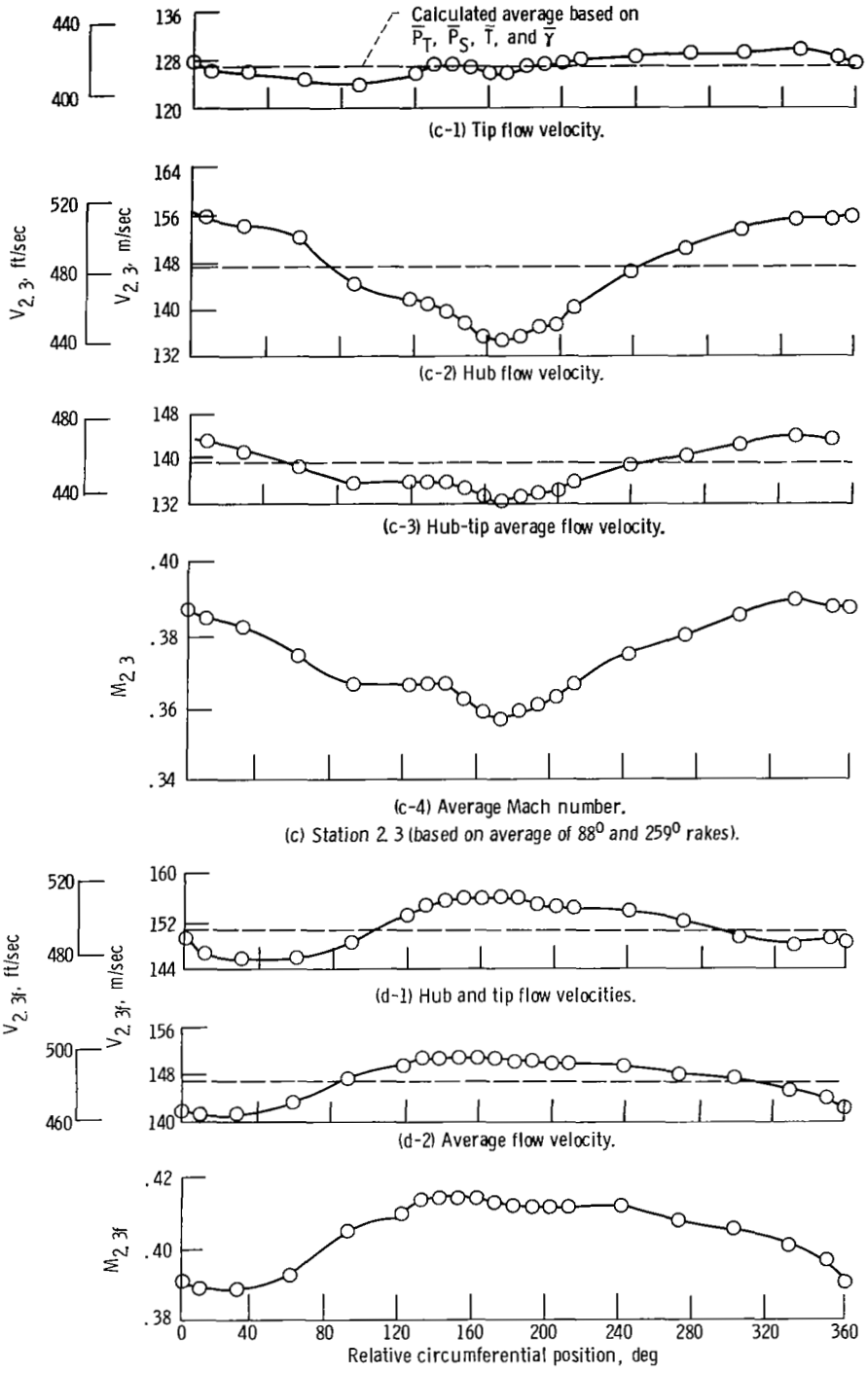

Figure 15. - Continued.

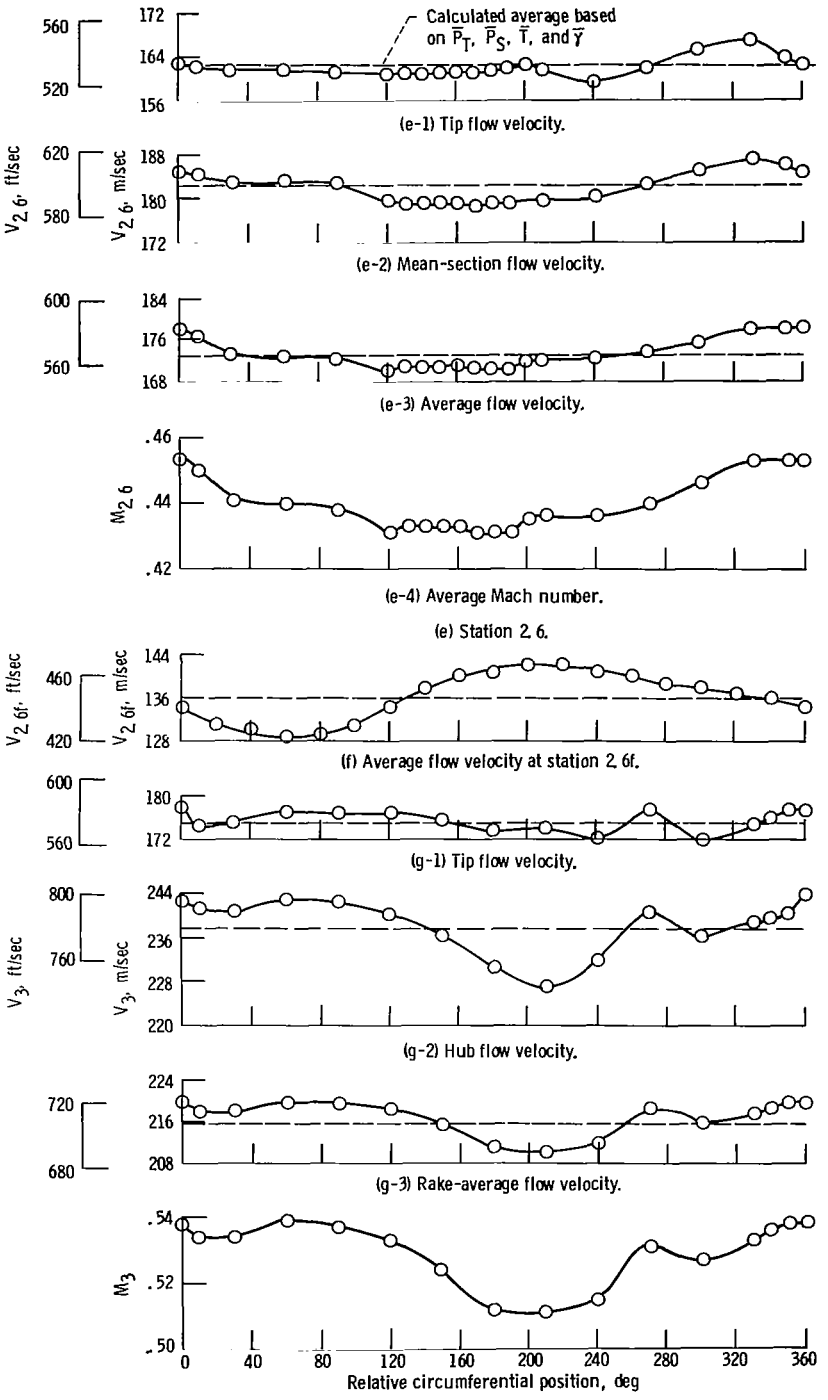

Figure 15. - Continued.

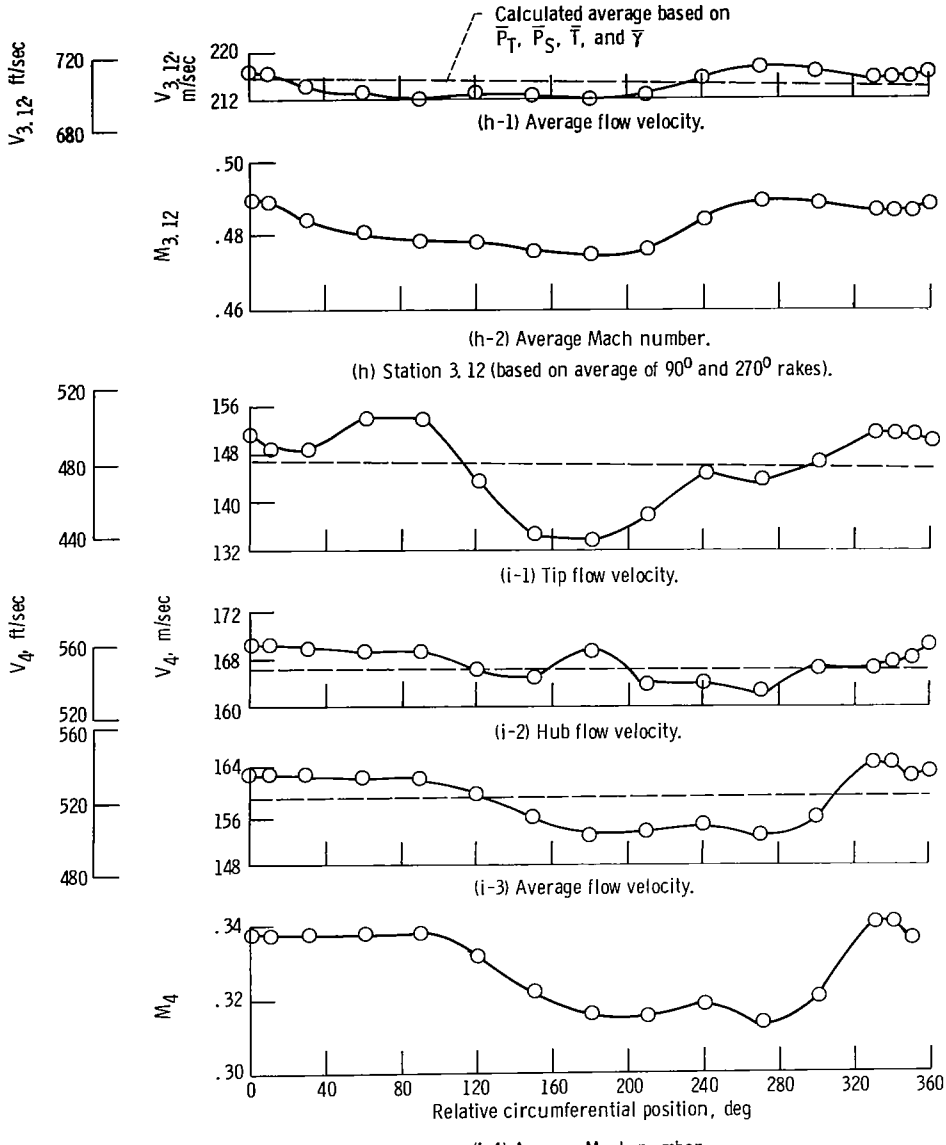

Figure 15. - Concluded.

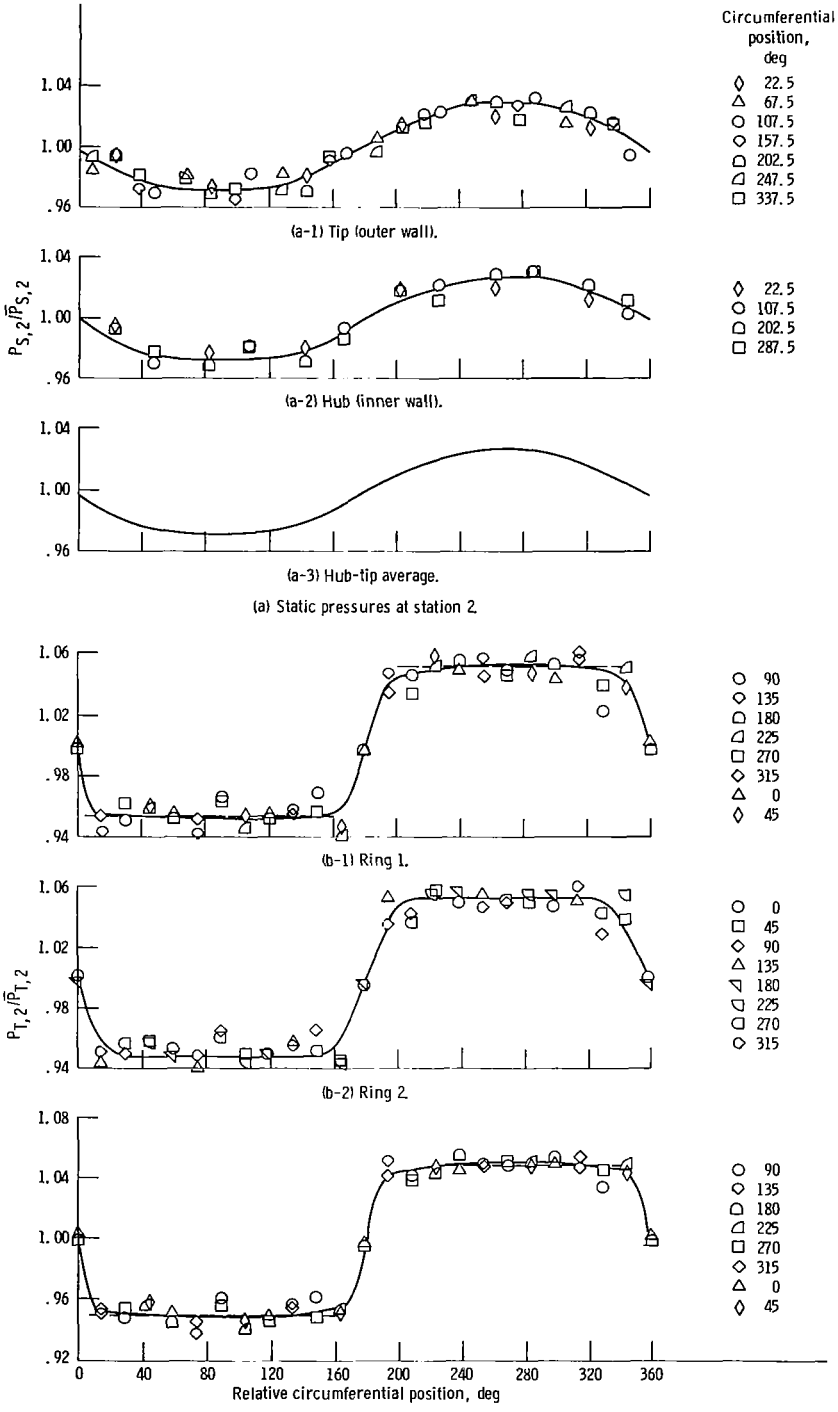

Figure 16. - Circumferential variation in total and static pressure for nominal low-speed-rotor speed of 8600 rpm.

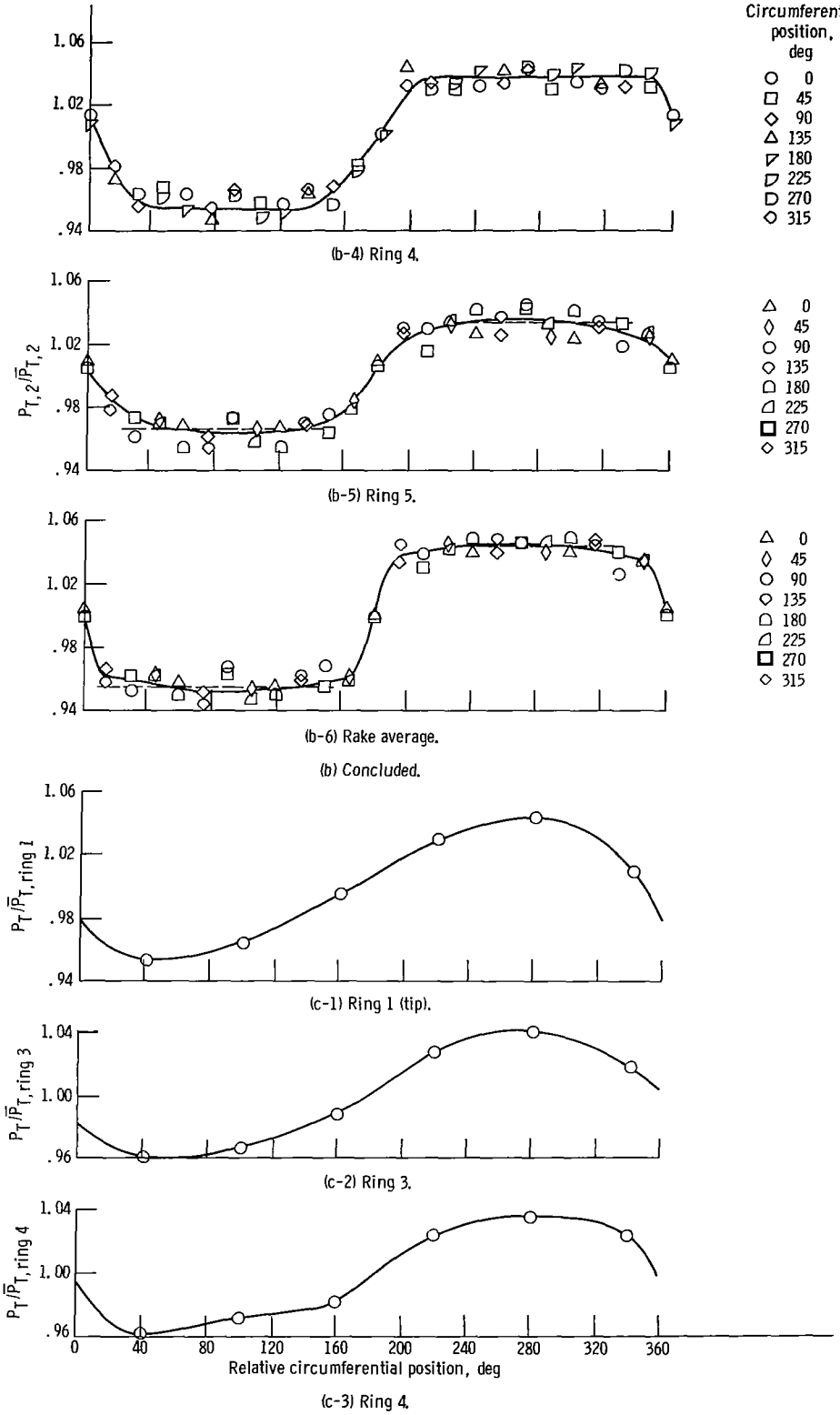

(b-4) Ring 4.

(b-5) Ring 5.

(b-6) Rake average.

(b) Concluded.

(c-1) Ring 1 (tip).

(c-2) Ring 3.

(c-3) Ring 4.

(c) Total pressures at station 2.1 (282° rake).

Figure 16. - Continued.

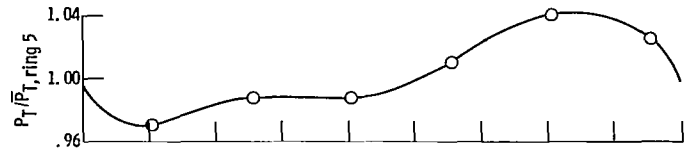

(c-4) Ring 5 (hub).

(c) Concluded.

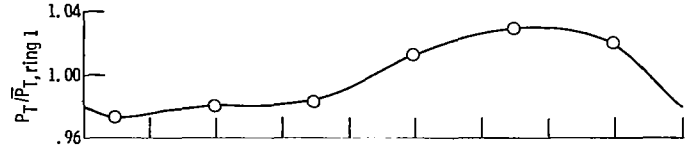

(d-1) Ring 1 (tip).

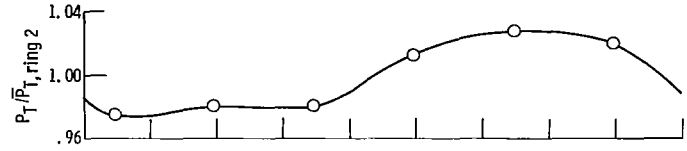

(d-2) Ring 2.

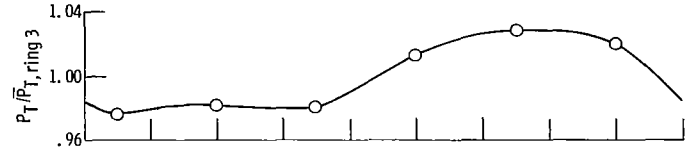

(d-3) Ring 3 (hub).

(d) Total pressures at station 2.3 (259° rake).

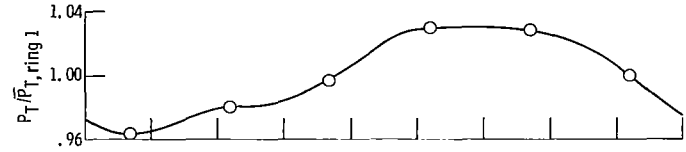

(e-1) Ring 1 (tip).

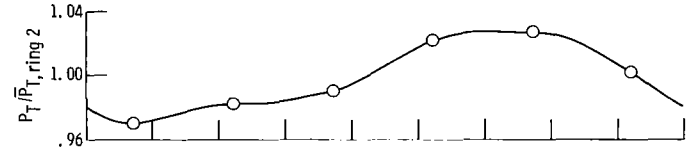

(e-2) Ring 2.

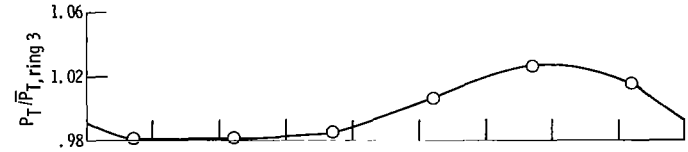

(e-3) Ring 3.

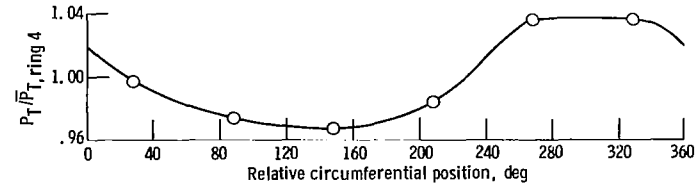

(e-4) Ring 4 (hub).

(e) Total pressures station 2.3 (88° rake).

Figure 16. - Continued.

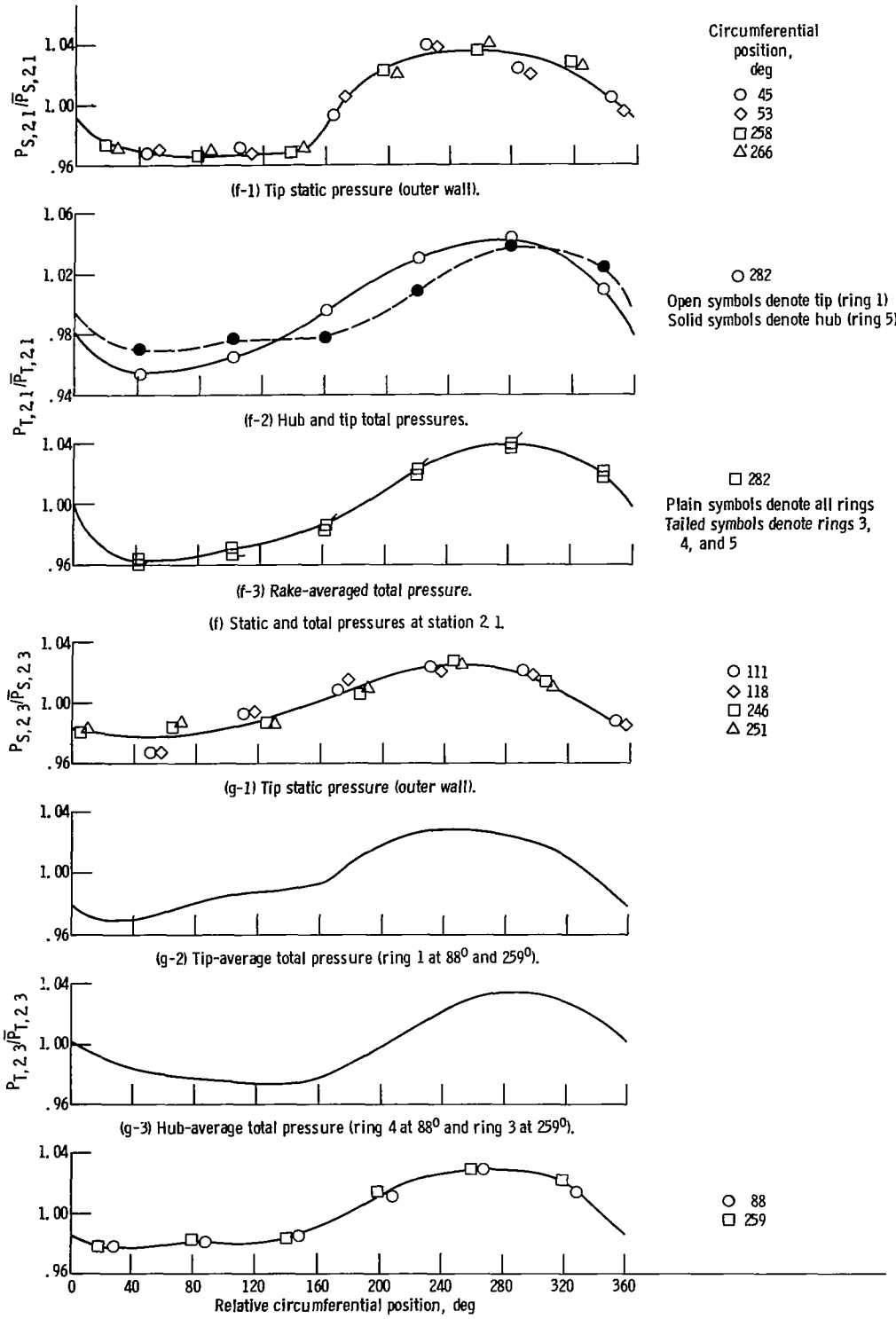

Figure 16. - Continued.

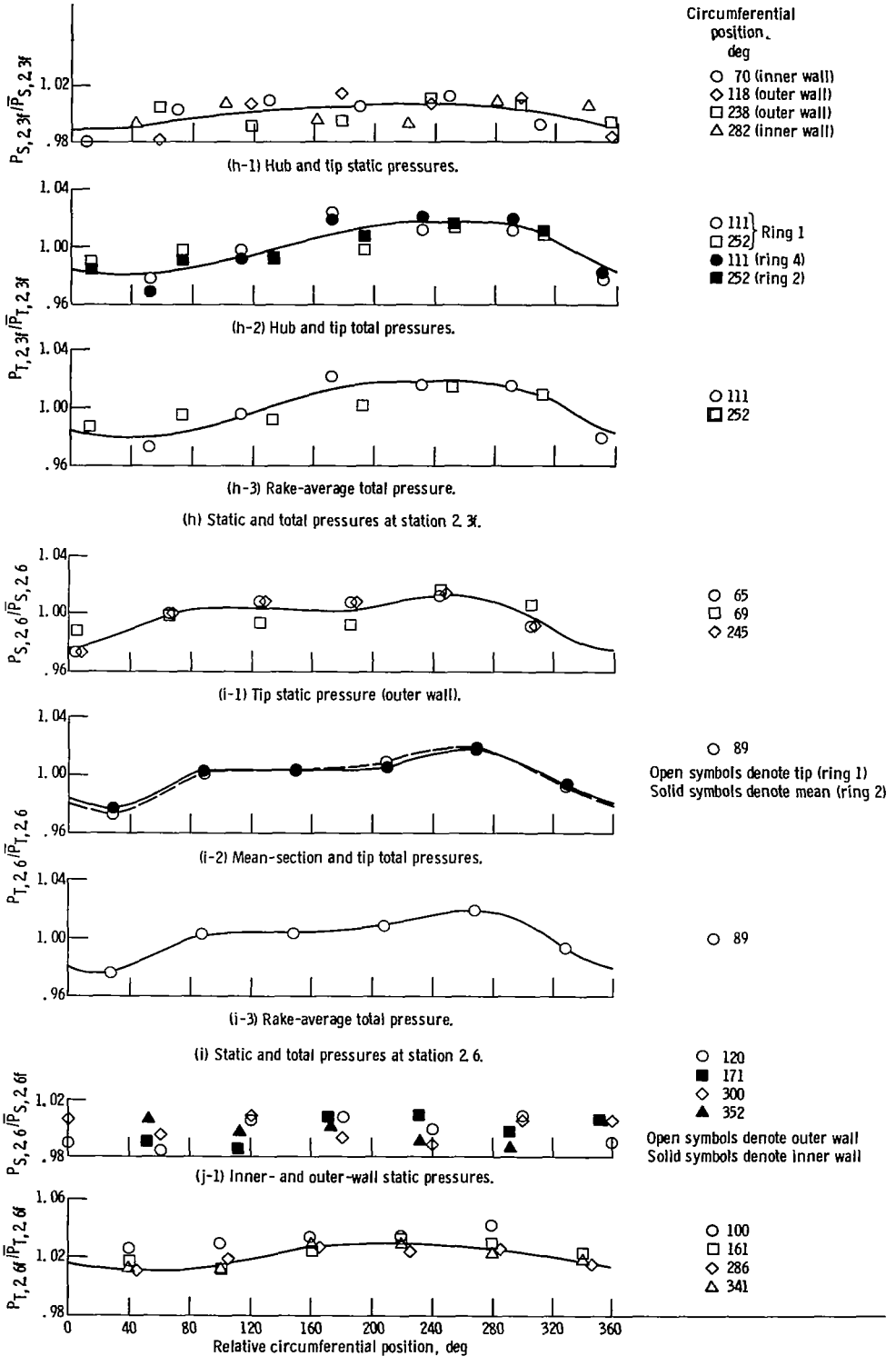

(h-1) Hub and tip static pressures.

(h-2) Hub and tip total pressures.

(h-3) Rake-average total pressure.

(h) Static and total pressures at station 2.3f.

(i-1) Tip static pressure (outer wall).

(i-2) Mean-section and tip total pressures.

(i-3) Rake-average total pressure.

(i) Static and total pressures at station 2.6.

(j-1) Inner- and outer-wall static pressures.

(j-2) Rake-average total pressure.

(j) Static and total pressures at station 2.6f.

Figure 16. - Continued.

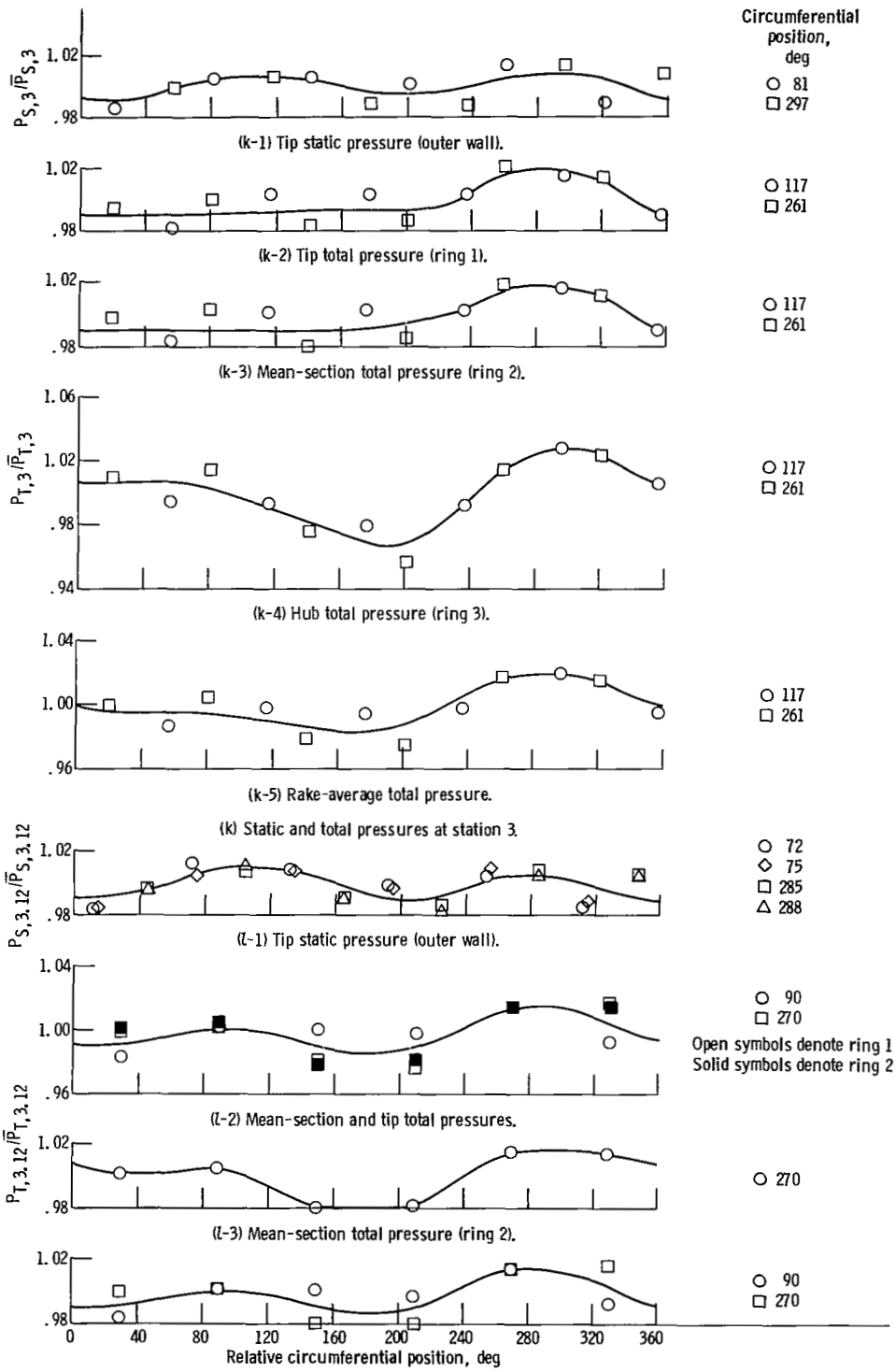

Figure 16. - Continued.

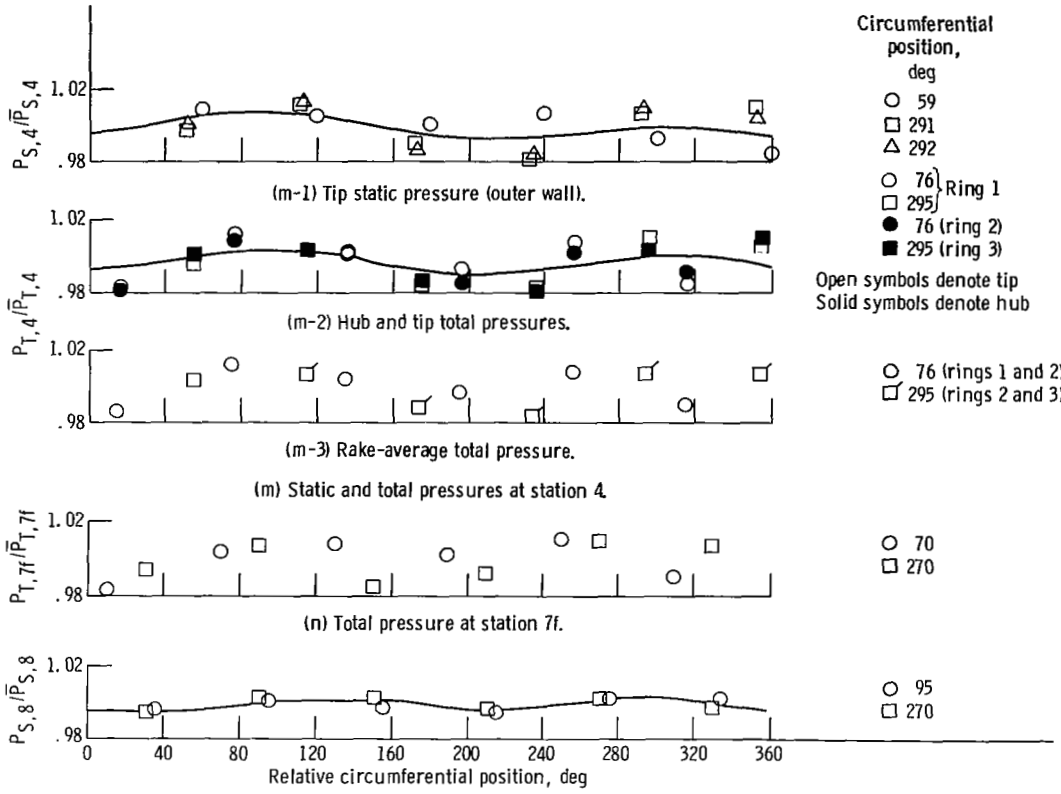

(m-1) Tip static pressure (outer wall).

(m-2) Hub and tip total pressures.

(m-3) Rake-average total pressure.

(m) Static and total pressures at station 4.

(n) Total pressure at station 7f.

(o) Static pressure at station 8.

Figure 16. - Concluded.

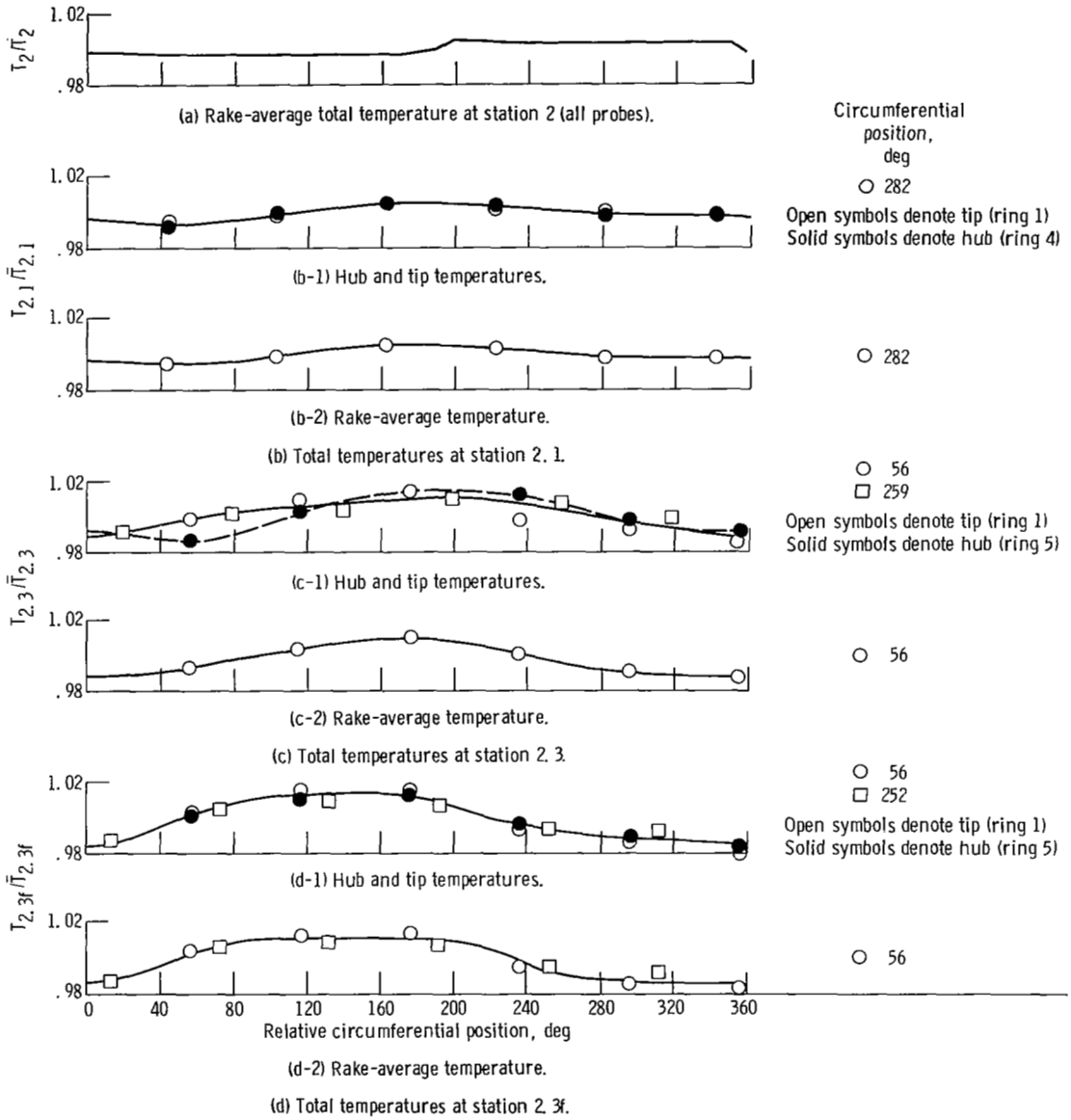

Figure 17. - Circumferential variation in total temperature for nominal low-speed-rotor speed of 8600 rpm.

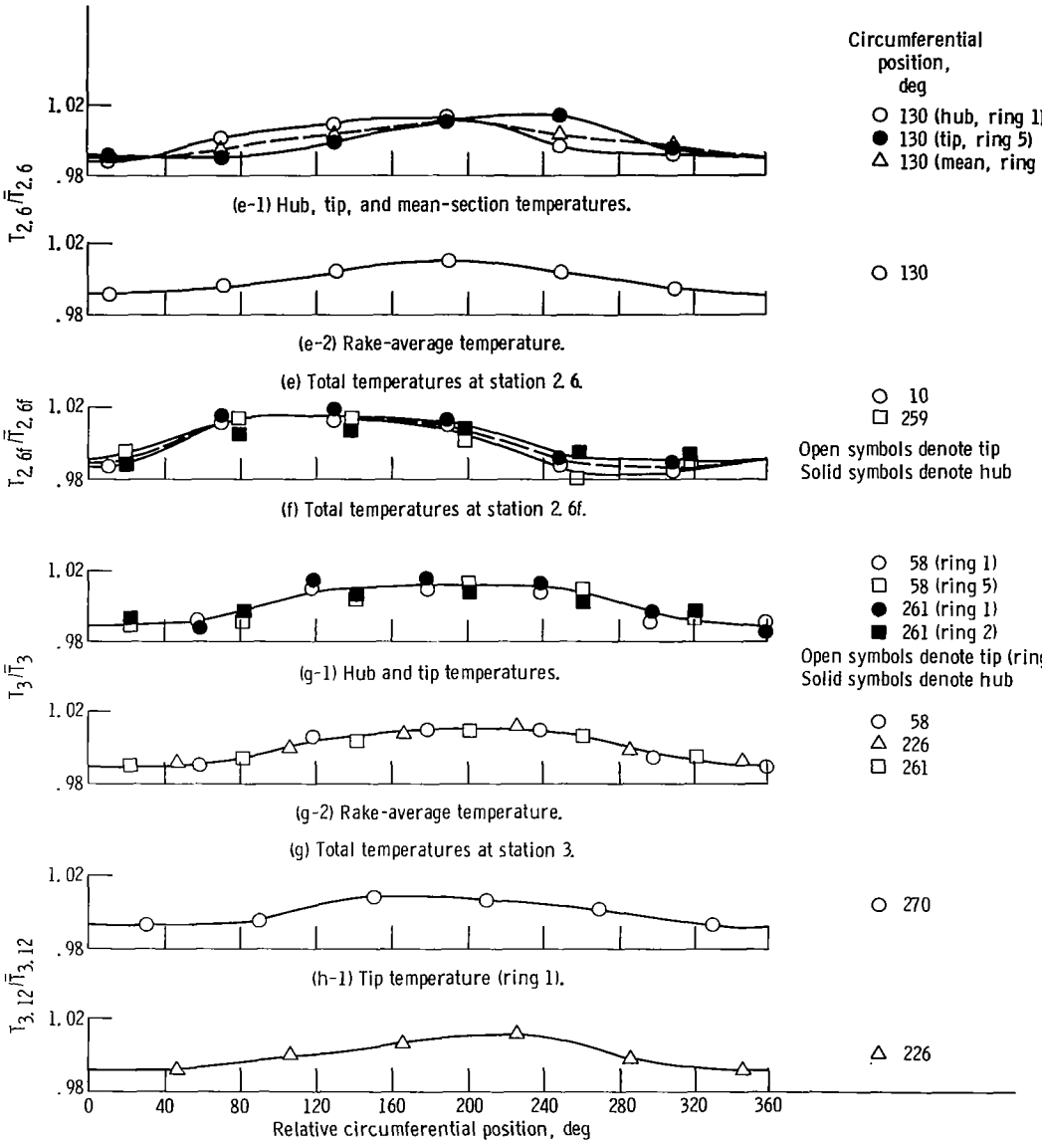

(e-1) Hub, tip, and mean-section temperatures.

(e-2) Rake-average temperature.

(e) Total temperatures at station 2.6.

(f) Total temperatures at station 2.6f.

(g-1) Hub and tip temperatures.

(g-2) Rake-average temperature.

(g) Total temperatures at station 3.

(h-1) Tip temperature (ring 1).

(h-2) Rake-average temperature.

(h) Total temperatures at station 3.12.

Figure 17. - Continued.

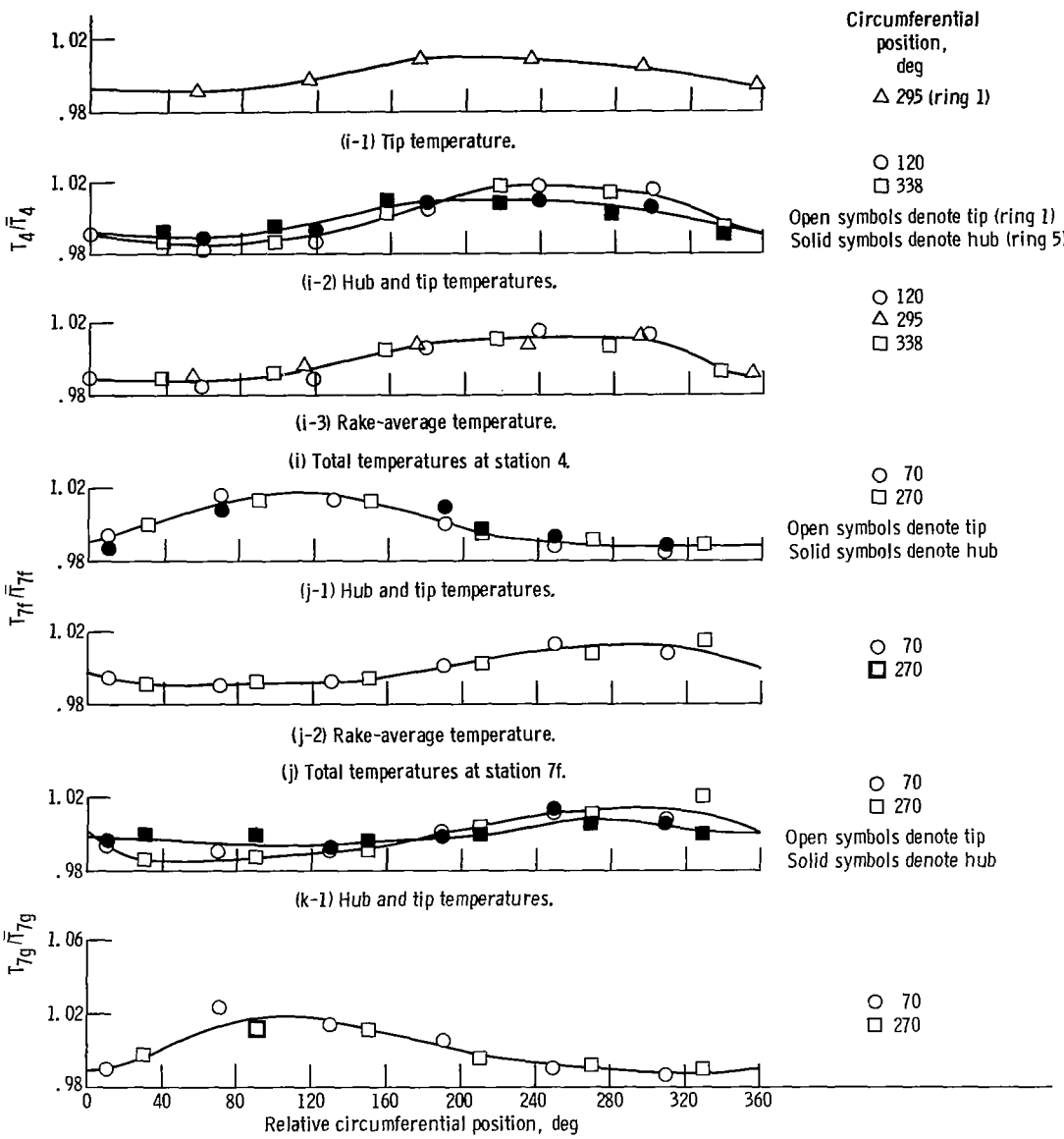

Figure 17. - Concluded.

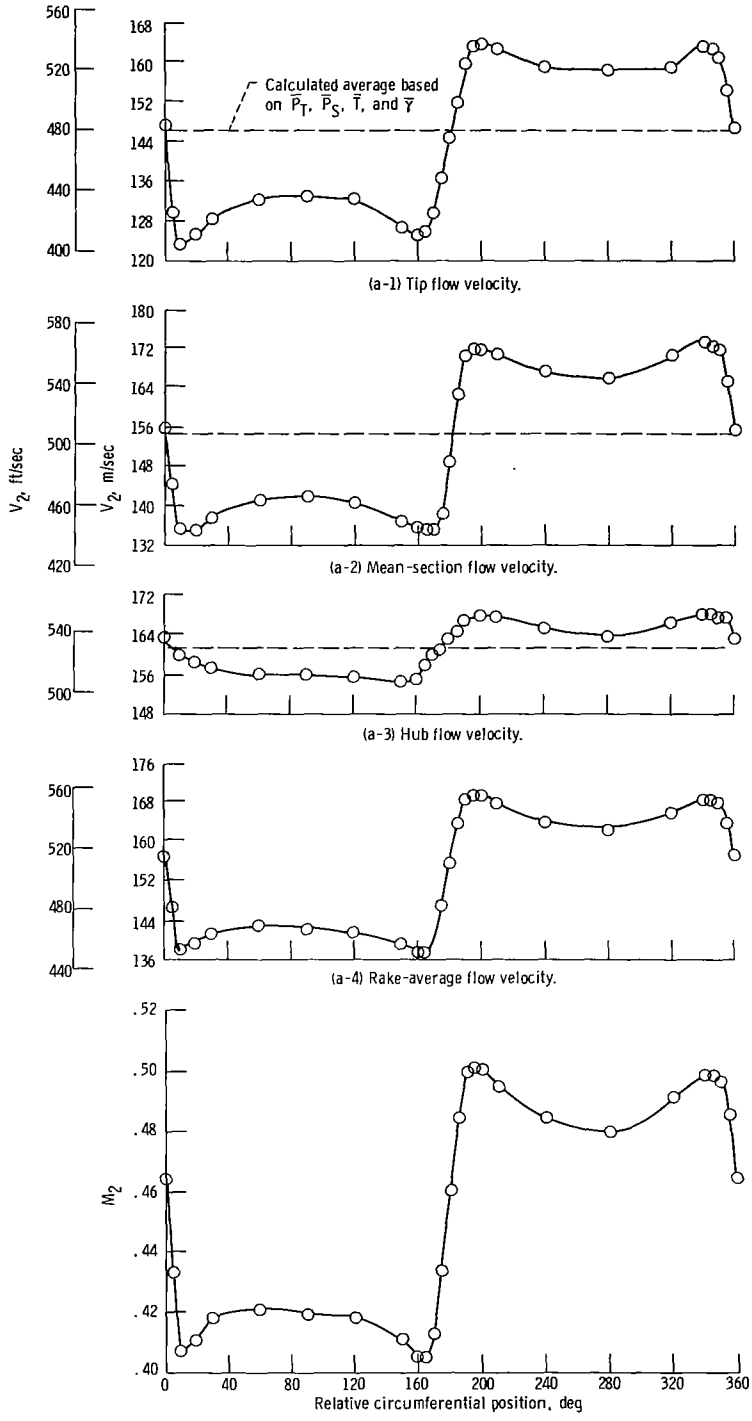

(a-1) Tip flow velocity.

(a-2) Mean-section flow velocity.

(a-3) Hub flow velocity.

(a-4) Rake-average flow velocity.

(a-5) Average Mach number.

(a) Station 2.

Figure 18. - Calculated circumferential variation in flow velocity and Mach number for nominal low-speed-rotor speed of 8600 rpm.

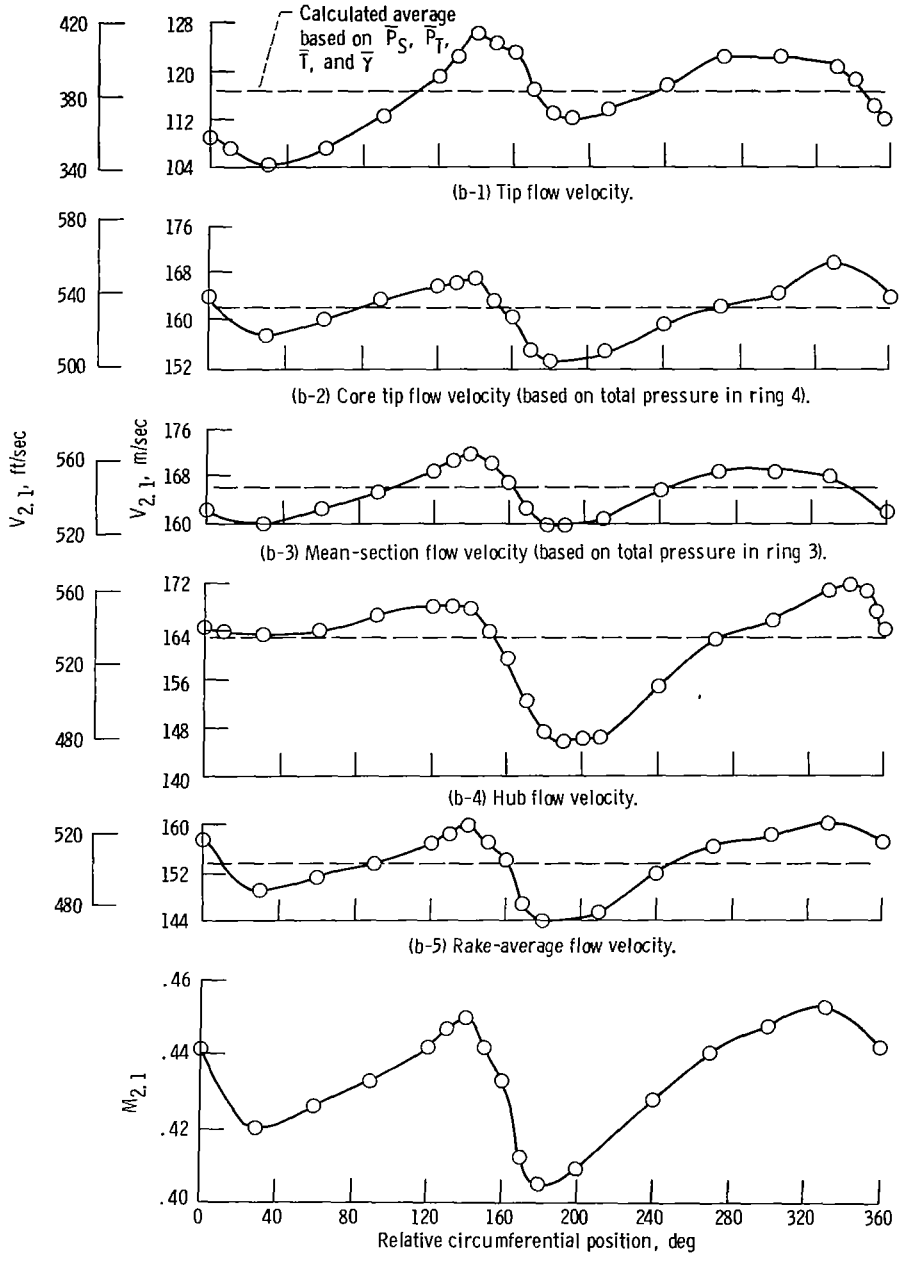

(b-1) Tip flow velocity.

(b-2) Core tip flow velocity (based on total pressure in ring 4).

(b-3) Mean-section flow velocity (based on total pressure in ring 3).

(b-4) Hub flow velocity.

(b-5) Rake-average flow velocity.

(b-6) Average Mach number.

(b) Station 2.1.

Figure 18. - Continued.

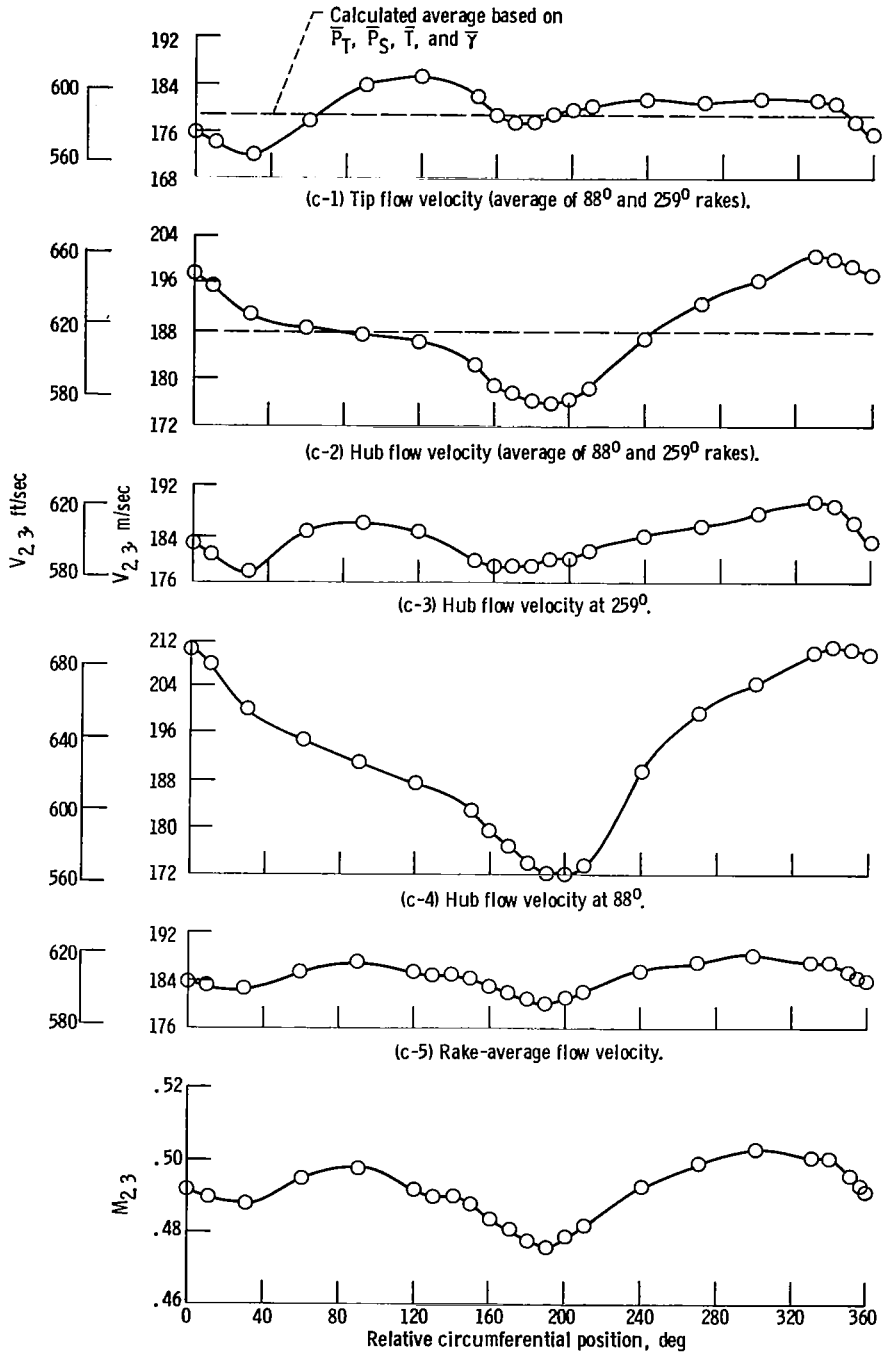

(c) Station 2.3.

Figure 18. - Continued.

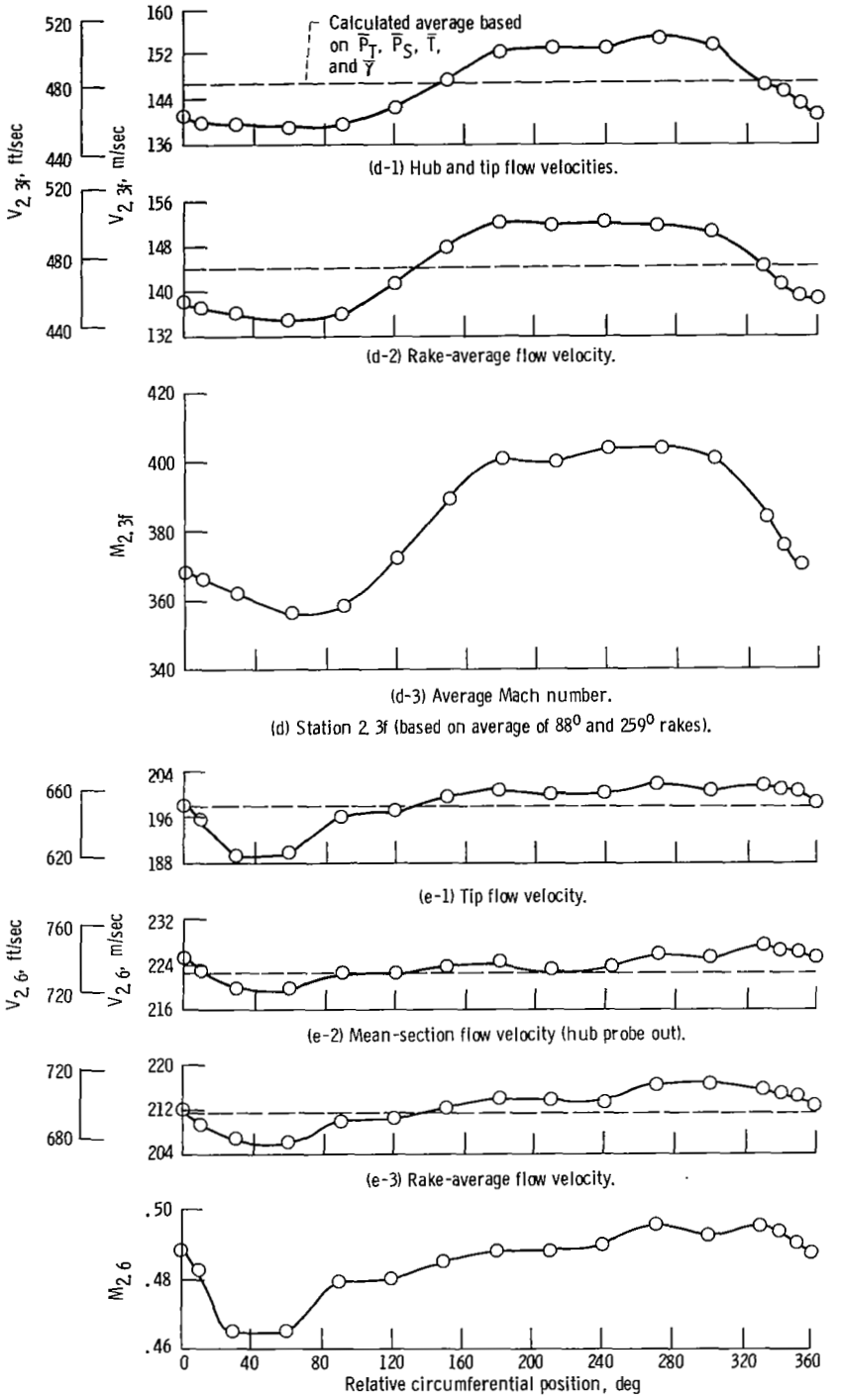

(d-1) Hub and tip flow velocities.

(d-2) Rake-average flow velocity.

(d-3) Average Mach number.

(d) Station 2.3f (based on average of 88^0 and 259^0 rakes).

(e-1) Tip flow velocity.

(e-2) Mean-section flow velocity (hub probe out).

(e-3) Rake-average flow velocity.

(e-4) Tip Mach number.

(e) Station 2.6.

Figure 18. - Continued.

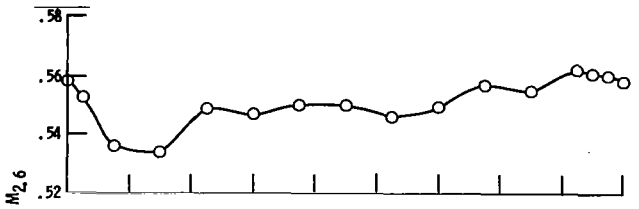

(e-5) Mean-section Mach number.

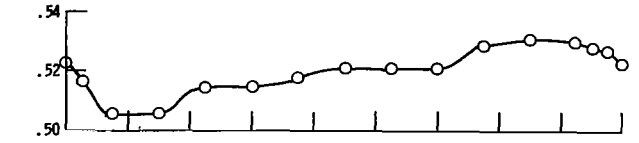

(e-6) Average Mach number.

(e) Concluded.

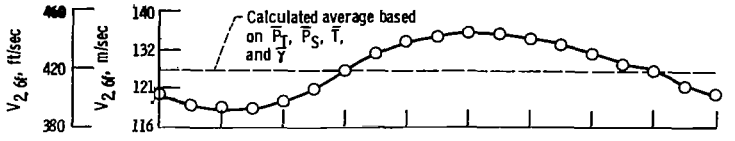

(f) Rake-average flow velocity at station 2.6f.

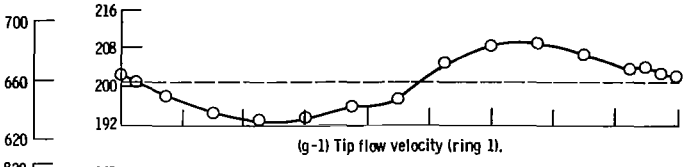

(g-1) Tip flow velocity (ring 1).

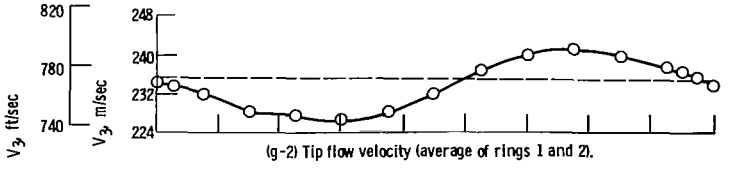

(g-2) Tip flow velocity (average of rings 1 and 2).

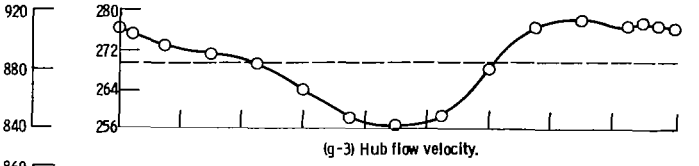

(g-3) Hub flow velocity.

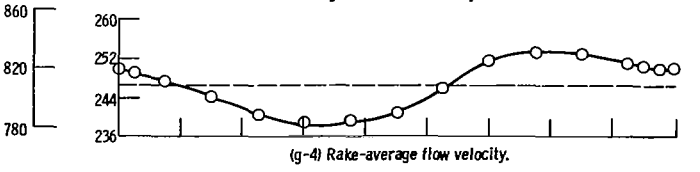

(g-4) Rake-average flow velocity.

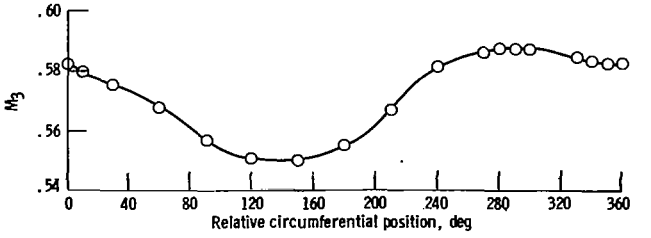

(g-5) Average Mach number.

(g) Station 3 (based on average of 117° and 261° rakes).

Figure 18. - Continued.

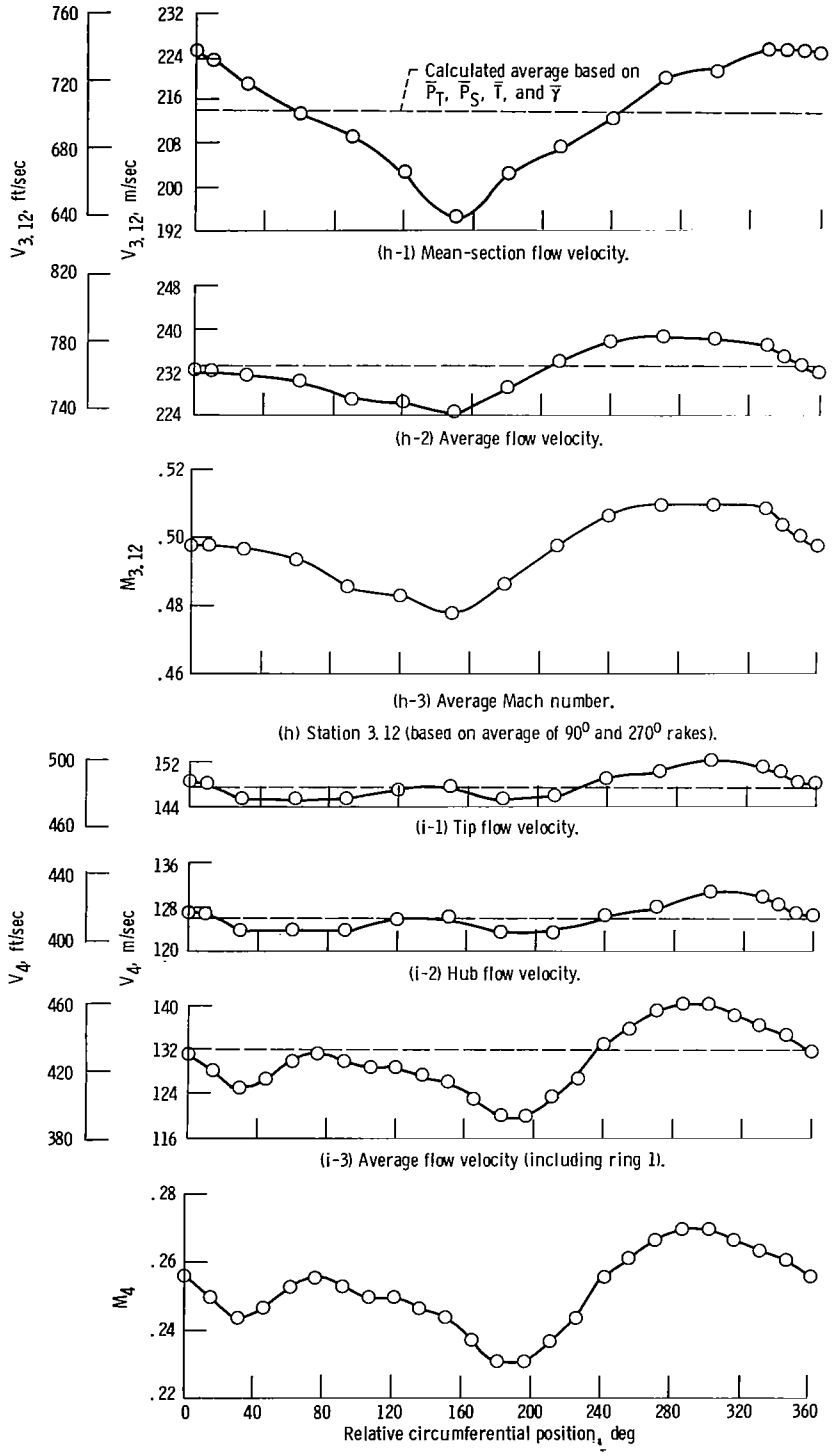

(h-1) Mean-section flow velocity.

(h-2) Average flow velocity.

(h-3) Average Mach number.

(h) Station 3.12 (based on average of 90^0 and 270^0 rakes).

(i-1) Tip flow velocity.

(i-2) Hub flow velocity.

(i-3) Average flow velocity (including ring 1).

(i-4) Average Mach number (including ring 1).

(i) Station 4 (based on average of 76^0 and 295^0 rakes).

Figure 18. - Concluded.

"The aeronautical and space activities of the United States shall be conducted so as to contribute . . . to the expansion of human knowledge of phenomena in the atmosphere and space. The Administration shall provide for the widest practicable and appropriate dissemination of information concerning its activities and the results thereof."

—NATIONAL AERONAUTICS AND SPACE ACT OF 1958

NASA SCIENTIFIC AND TECHNICAL PUBLICATIONS

TECHNICAL REPORTS: Scientific and technical information considered important, complete, and a lasting contribution to existing knowledge.

TECHNICAL NOTES: Information less broad in scope but nevertheless of importance as a contribution to existing knowledge.

TECHNICAL MEMORANDUMS: Information receiving limited distribution because of preliminary data, security classification, or other reasons. Also includes conference proceedings with either limited or unlimited distribution.

CONTRACTOR REPORTS: Scientific and technical information generated under a NASA contract or grant and considered an important contribution to existing knowledge.

TECHNICAL TRANSLATIONS: Information published in a foreign language considered to merit NASA distribution in English.

SPECIAL PUBLICATIONS: Information derived from or of value to NASA activities. Publications include final reports of major projects, monographs, data compilations, handbooks, sourcebooks, and special bibliographies.

TECHNOLOGY UTILIZATION PUBLICATIONS: Information on technology used by NASA that may be of particular interest in commercial and other non-aerospace applications. Publications include Tech Briefs, Technology Utilization Reports and Technology Surveys.

Details on the availability of these publications may be obtained from:

SCIENTIFIC AND TECHNICAL INFORMATION OFFICE

NATIONAL AERONAUTICS AND SPACE ADMINISTRATION

Washington, D.C. 20546